Aerodynamic and Flight Dynamic Simulations of Aileron Characteristics

Erkki Soinne

Department of Aeronautics
Royal Institute of Technology
SE-100 44 Stockholm, Sweden

Report 2000-12
ISSN 0280-4646

Dissertation for the degree of Doctor of Technology to be presented with due permission for public examination and debate in Auditorium L1 at Royal Institute of Technology, Drottning Kristinas väg 30, Stockholm on November 24th 2000, at 1:15 pm.

ABSTRACT

The subject of this investigation is the application of CFD computations to flows around airplane ailerons combined with flight mechanical simulations to study the impact on airplane rolling maneuvers and aileron dynamics. The practical application is on Saab 2000 commuter airplane.

In the validation of CFD computations the low speed airfoils FX 61-163 and FX 66-17AII-182 were investigated with the 2D Navier-Stokes code ns2d by comparing the computations with selected wind tunnel experiments. The medium speed MS(1)-0313 and the transonic DLBA032 airfoils with plain ailerons were investigated with ns2d and NSMB codes in selected wind tunnel cases representative for the ailerons of Saab 2000 aircraft. One algebraic and three k-ε turbulence models were used in the calculations at different aileron deflections. The effects of local mesh refinement and grid convergence were studied on the aerodynamic coefficients.

Two-dimensional CFD computations were made on Saab 2000 aileron to compare the hinge moment with flight test results, measured by disconnecting the left and right hand side ailerons. The local angles of attack were determined by using extended lifting line theory and the conversion to 3D coefficients was made with handbook methods. The airplane rolling moment was determined by inserting the CFD derived lift effectiveness into the calculations.

The effects of aileron slot and tab slot gap sizes as well as aileron hinge axis position on the aerodynamic coefficients were computed with the ns2d code. The CFD derived aerodynamic coefficients were fed into a six degree of freedom flight mechanical simulation system to study the impact on airplane rolling maneuvers. Frequency analysis was performed on the response of aileron deflection, airplane roll rate and roll acceleration to applied wheel force using fast Fourier transform, spectrum analysis and system identification.

A review was made on practical aileron design considerations with issues on maximum wheel force, aileron effectiveness, wind tunnel testing, induced drag and aileron control system.

PREFACE

This research work on aerodynamically balanced control surfaces was performed in a collaborative research project between Saab Aerospace/Saab Aircraft AB and Department of Aeronautics at Royal Institute of Technology and run within the competence center PSCI (Parallel and Scientific Computing Institute) at Royal Institute of Technology (KTH). Financial support for this work by Saab Aerospace/Saab Aircraft AB and by NUTEK, the Swedish National Board for Industrial & Technical Development, provided under the auspices of PSCI, is gratefully acknowledged.

The use of the Cray T3E and C90 computers of the National Supercomputer Centre in Sweden at Linköping University is gratefully acknowledged. Also the use of the computers at the Center for Parallel Computers (PDC) at Royal Institute of Technology (KTH) is gratefully acknowledged. Altogether over 16000 hours of CPU time was utilized in this investigation.

The work was initiated by Tommy Nygren, then Manager of Aeronautical Engineering at Saab Aircraft AB, now the Technical Director. When the production of civil aircraft was terminated at Saab his support was crucial for completing the research program. I am grateful for his support during the project. The work was done at Saab under the supervision of Wim Willemse, Manager of Aerodynamics and Stability and Control. He has shared his experience in aerodynamics and stability and control, gained at Fokker, and greatly improved the reports by thorough checking and constructive comments. Professor Rizzi, my supervisor at the Department of Aeronautics at Royal Institute of Technology, has shared his knowledge in aerodynamics and CFD. I am grateful for his valuable advice on CFD and his enthusiasm and support during the project. I am also grateful that my both supervisors, in spite of their genuine interest in the subject, have let me work largely independently. The help that was obtained from the Department of Aeronautics at Royal Institute of Technology, NSMB consortium and Saab is gratefully acknowledged. Special thanks go to the CFD group of Saab for their support when problems were found in ns2d code. Finally, I wish to acknowledge the encouragement provided by my fiancee Ulla who has also checked the language of the thesis.

CONTENTS

1. INTRODUCTION

Mechanically controlled ailerons are used on general aviation aircraft and together with an aerodynamic balance on up to 150 passenger commercial aircraft, because a mechanical control system provides large potential in cost savings. It has been estimated that on Saab 2000 commuter aircraft, shown in fig. 1, the cost increase due to a powered elevator control system was over 1% of the airplane 12 million dollar sales price. Because the market situation sets the airplane pricing the manufacturer has to stand for the extra cost. If the manufacturer´s profit is say 10% of the airplane selling price the extra cost will consume over 10% of the profit.

However, a mechanically controlled aileron has a higher development risk due to uncertainties in the aerodynamics around the balance. This was noticed in the development of the roll control for Saab 2000. Even though the control system was based on the smaller Saab 340, difficulties were experienced due to more stringent certification requirements and the larger size and speed of 2000. Common problems for aerodynamically balanced ailerons are high wheel forces at high speed and a tendency to overbalance in sideslips flaps deflected. With a very high balancing ratio production tolerances may cause wheel force variations. To increase the know-how and reduce the future development risk a collaborative research project on aerodynamically balanced control surfaces was started between Saab Aerospace/Saab Aircraft AB and the Department of Aeronautics at Royal Institute of Technology. This thesis is a results of the research project.

On aircraft with mechanical control systems there is usually a slot between the control surface and the fixed part of the airfoil. The flow conditions in the slot are dependent on

Figure 1. Saab 340 and 2000 commuter aircraft.

the slot geometry, Reynolds number and Mach number. This makes it a demanding task to find a control surface geometry that gives the pilot acceptable control forces in the entire speed regime.

Reaching the correct Mach and Reynolds numbers is not easy in wind tunnel tests but it would require a pressurized tunnel. Flight tests provide the correct conditions but are expensive and possible only at a late stage of an aircraft project. CFD is a new method to study the aerodynamics of control surfaces. Compared with testing it is easy to vary the flow conditions and the geometry. Hence one main idea is to investigate the application of CFD computations to flows around ailerons. The computed aerodynamic coefficients are however only intermediate results and do not tell if an aileron configuration fulfills the appropriate certification requirements. Consequently another main idea of this work is to link the CFD derived aerodynamic coefficients with a flight mechanical simulation model. By performing simulations in dimensioning flight cases it is possible to assess the performance of an aileron configuration. The thesis consists of aileron control system design based on CFD computations, flight mechanical simulations and practical design experience. The publications and reports written within this work are outlined in chapter 2.

Published literature on aileron design is limited as shown by the performed literature survey (ref. 60). Out of the over hundred references found on aileron aerodynamics only a small amount deals with aileron design. There are descriptions on the development of manual controls with aerodynamic balancing on following airplanes:

Airplane	reference	year
Douglas DC-6	19	1949
Fokker F28	4	1969
Aeritalia G 222	27	1972
Dornier 228	28	1983
Pilatus PC-9	39, 40	1988
Aermacchi AMX, MB-326/329	7	1990

However, only the references on Pilatus PC-9 are entirely devoted to the design of roll control. In the literature survey there is a list of 35 selected internal Saab reports (out of several hundreds reports and memos) on the roll control development of Saab 2000.

The general principles of control surface design were developed already before and during the second World War. The experience gathered in Great Britain was documented by Morgan and Thomas in the classical paper of ref. 46. This paper already describes the problems with production variability causing variation in control surface hinge moment. A comprehensive paper on spring tab controls (ref. 45) was published by Morgan, Bethwaite and Nivison summarizing the experience gained at RAE. A classical paper by Morris (ref. 47) treats the implications of icing on hinge moment coefficient and amount of balance. The research work on lateral control design, conducted at NACA in the United States, was summarized by Toll after the war, see ref. 64.

There are tens of reports on aerodynamic data of control surfaces, most of which date back to the 40´s. The classical theory by Glauert of a thin airfoil with a hinged flap is presented in ref. 29. However, viscous effects strongly dominate the flow around a control

surface and simple analytical theory is not sufficient in general. Semi empirical methods, taking into account the effects of boundary layer, are available in ESDU (ref. 22) and DATCOM (ref. 65). These methods are based on a large number of wind tunnel tests conducted on different geometries such as plain aileron, overhang balance, internal (Irving) balance and Frise aileron including the effects of gap and beveled trailing edge. The general trends of the different geometries on aileron hinge moment and lift are summarized in refs. 53 and 64. However, the references warn that the trends may not be valid for modern airfoil sections differing from those employed in the experiments. The only possibility to obtain data for modern, for example rear loaded sections is to conduct new wind tunnel tests or perform CFD computations. Only recently there have been efforts reported, see refs. 30 and 31.

Originally the intention of this work was to concentrate on the applied aerodynamics and flight dynamics of ailerons and not to deal with CFD code development and validation. However, it was soon obvious that this could not be avoided. The person responsible for the ns2d code had left the company and another had taken over the program with only a limited documentation of the source code files. Changes were made into the code without comprehensive testing leading twice to the situation that the previously successful runs on the FX 61-163 airfoil unexpectedly crashed. This led to a long period of corrections and testing and a delay of 12 months. During the last phase of the computations it was noticed that the results depended on which computer was employed for the computations. Grid convergence had never been investigated either. All this meant that a considerable effort was spent on validation to ensure that the obtained results are trustworthy.

Validation of CFD codes is a delicate matter. Every large code contains errors and discrepancies. Even a theoretically fault free code has inherent limitations due to simplifications in governing equations of the flow and solution methods. By successfully testing an arbitrary flow case it is not possible to draw the conclusion that a program is good for any other flow case. Code verification, validation, certification and calibration have drawn increased attention in the past years. The terminology has been developing but it still seems to be somewhat varying between the authors. Quite a number of papers has been presented, of which reference 48 by Rizzi and Vos and number 49 by Roache are two examples. Following these the word validation is here used for validation of calculations by comparing computed results with trustworthy experimental measurements. Published wind tunnel experiments for the validation of CFD computations are rare. The afore mentioned literature survey, performed through the NASA database and internal sources at Saab, produced only one low speed (ref. 69) and one high speed experiment (ref. 10) suitable for code validation on ailerons.

Comparison of computations with experimental results usually shows some discrepancy. This may be due to acknowledged and unacknowledged errors in modeling and simulation. Examples of the former are approximations in the modeling of the physics and round-off errors in the computations. A human programming error is an unacknowledged error. Common for errors is that they do not arise due to lack of knowledge which, on the contrary, is the case for uncertainties. For example lack of knowledge about the complex phenomenon of turbulence enforces to apply simplifications in turbulence models with associated uncertainties. Also experiments contain uncertainties such as the geometrical dimensions of a model and the measuring accuracy. Therefore the whole process of validation is related with some uncertainty.

The first step in the investigation is the analysis of a well known single element airfoil to obtain confidence in the code used. The classical laminar airfoil FX 61-163, designed by F.X. Wortmann, was chosen here. To get an idea on the accuracy of a code on airfoil analysis at least one full set of lift, drag and pitching moment coefficients has to be computed. This has never been done before with the ns2d code used at Saab, but due to the tedious calculations only individual points on a polar had been computed in the past. The complete polar up to maximum lift coefficient was computed at one Reynolds number transition free. Two polars were computed at different Reynolds numbers with fixed transition. Two turbulence models were used in the computations; a two-layer k-ε model and a modification of it with an eddy viscosity limiter. These computations were made on a mesh with zero trailing edge thickness modeling the nominal airfoil contour. The computed lift and pitching moment curves somewhat deviated from the measurements why the effect of the trailing edge geometry was studied with the MSES code (ref. 16). An outline of the work of the first part is presented in chapter 3.

Due to the uncertainties on the trailing edge geometry of the FX 61-163 airfoil in the experiments another well-known single element airfoil was studied. FX 66-17AII-182 airfoil was chosen because wind tunnel tests, performed in NASA low turbulence tunnel in Langley by Somers (ref. 63), were available also including a measurement on the model geometry. The wind tunnel model had a blunt, finite thickness trailing edge. The computations were performed with the renewed ns2d code using the two-layer k-ε turbulence model with an empirical transition model. The transition model permitted comparisons with experiments at Reynolds numbers in which transition locations were not measured. The computed lift, drag and pitching moment coefficients are compared with existing wind tunnel data in chapter 3.

It is known that in two-dimensional flow lift is produced in potential theory only if the stream lines are forced to leave the trailing edge smoothly. This can be done by prescribing the so called Kutta condition at the airfoil trailing edge. On an airfoil with a finite trailing edge angle (e.g a Kármán-Trefftz airfoil) a stagnation point is formed at the trailing edge. On an airfoil with zero trailing edge angle (e.g a Joukowsky airfoil) there is no stagnation point, but the velocities on the upper and lower surfaces of trailing edge are equal. The effect of inertia is included in Euler equations and Kutta condition is not needed for the computation of lift when the airfoil has a trailing edge with a sharp corner. The effect of viscosity is introduced with Navier-Stokes equations and should potentially improve the analysis as viscous phenomena appear in the wake aft of the airfoil trailing edge. Hence the analysis of the flow conditions at the trailing edge has a coupling to the creation of lift, a classical question in aerodynamics. On ailerons the flow conditions are especially important, because the aileron hinge moment is strongly influenced by the long moment arm stretching from the trailing edge to the hinge axis.

In the next step computations were made with two codes, ns2d and NSMB, in test cases representative for the ailerons of Saab 2000 aircraft. Because there are no available wind tunnel measurements on a two-dimensional airfoil with a balanced aileron, airfoils with slotted plain ailerons were used at low (ref. 69) and high speeds (ref. 10). However, one has to keep in mind that a balanced aileron has a hinge moment coefficient with an order of magnitude of 0.01 whereas for a plain type aileron the order of magnitude is 0.1. This means that one has to create the grids so accurately that they are good also for a balanced aileron. Special attention must be paid on the trailing edge as the fulfillment of the Kutta condition and the hinge moment coefficient may be sensitive in this region due to

the long moment arm. Both proper mesh generation and run strategies to guarantee converged runs on airfoils with balanced control surfaces must be investigated. If the mesh is too coarse the runs may converge as such but utilization of a finer mesh may change the results. In this case one cannot speak about mesh convergence. When a sufficiently fine mesh is used the runs must be so long that the results do not change anymore. When grid convergence and converged runs have been reached the computed results shall be compared with measured values.

The low speed test case is the MS(1)-0313 airfoil with a 20% chord slotted plain aileron deflected at -10^o, 0^o and $+10^o$. Computations with ns2d were made with Baldwin-Lomax, Launder-Sharma and two-layer turbulence models and with NSMB code the Baldwin-Lomax and Chien´s k-ε turbulence models were used. The validation test cases were chosen so that they represent the dimensioning cases for ailerons at low speed flight. The computed results on lift, drag, pitching moment and hinge moment coefficients are compared with experimental values in chapter 4.

The case of high speed flight was also studied using the same set of turbulence models. The McDonnel Douglas transonic airfoil DLBA032 with a 25% chord plain aileron was analyzed with a control surface deflection of $+5^o$. The angle of attack was chosen so that the lift coefficient with zero aileron deflection matched the local lift coefficient at Saab 2000 aileron at demonstrated flight diving speed V_{DF}/M_{DF}. Because the aileron was fixed with a bracket in the wind tunnel tests the hinge moment was not measured but instead a comparison on pressure distribution was made.

Not only the basic grids but also grid variation studies were undertaken on MS(1)-0313 airfoil with aileron deflection $+10^o$ in the low speed test case with ns2d code by refining the grid locally, relaxing the first cell size and increasing the computational domain size. Grid convergence was studied with the help of the basic mesh that was created with multiples of 4 cells in every subface giving three grid levels denoted as coarse, medium and fine mesh levels. A very fine mesh was created separately by once more doubling the number of cells in the two directions. Results at infinitely dense grid level were determined by using Richardson´s extrapolation.

When the grid generation methodology was established the Saab 2000 type design aileron was modeled at two sections and computations were made at five aileron deflections in a selected flight test case. The methodology used was to determine the local angle of attack at the aileron sections with an extended lifting line program LIFLI. Local lift and hinge moment coefficients were then computed with the ns2d code. The three-dimensional airplane rolling moment and aileron hinge moment coefficients were determined using the handbook methods of ESDU. Computed hinge moment and rolling moment coefficients are compared with flight test values in chapter 5, where also a review on practical design experience is made. The effect of production tolerances was studied by performing CFD computations on aileron geometries with a variation on aileron and tab slot gap sizes within the allowable minimum and maximum values. Also the aileron hinge axis location was varied between the typed design and the original lower positions.

The inhouse simulation system FORMIC in use at Saab was employed for the flight mechanical simulations on Saab 2000 and 340 aircraft. The aircraft models, linked together with FORMIC, are based on state space representation of the flight mechanical six degree of freedom differential equations and the aircraft systems. Simulations were per-

formed in steady heading sideslips in a flight test case at maximum flaps extended speed V_{FE}. The simulations were performed for the type design aileron geometry and for the aileron without vortex generators, based on CFD derived aerodynamic data.

Roll maneuvers were studied in one low and one high speed case. In the low speed case roll control efficiency was investigated at the reference speed for landing V_{REF} in landing configuration. In the high speed case roll control efficiency was investigated in an en-route condition at airspeeds up to the maximum speed during normally expected conditions of operation V_{MO}/M_{MO}. The roll maneuvers were studied using the type design gear tab configuration and also a tentative spring tab configuration. Also the effect of production tolerances was investigated. Simulations were performed on the effect of the aileron slot gap size and the misrigging of the tab. The results are presented for both the type design geared tab and the spring tab systems in chapter 6.

Frequency analysis was used to study the response of aileron deflection, airplane roll rate and roll acceleration to the wheel force applied by the pilot. The applied wheel force was modeled using a chirp signal with varying frequency. The response of the system in time was determined with the FORMIC simulation system that produces the output signal at selected discrete time steps. The frequency response was calculated using Fourier analysis, spectrum analysis and system identification employing an ARX model.

The frequency response of the aileron and airplane motion to the applied wheel force was determined for Saab 340 and 2000 type design configurations in approach flight conditions at the lowest value of minimum control speed in landing when the airplanes are most susceptible to gusts. Computations were also made on the effects of flying speed, airplane rolling moment of inertia, aileron control path stiffness as well as setting the aileron control system friction and damping to zero. Simulations on Saab 2000 without vortex generators were made with pertinent aerodynamic data and by introducing the aileron hinge moment and airplane rolling moment from the CFD computations. The computed results of the flight dynamic simulations and the frequency analysis are presented in chapter 6.

2. DOCUMENT STRUCTURE

This PhD thesis consists of an overview and the selected six papers based on a number of reports forming the following structure:

Paper I:
Soinne E., Navier-Stokes Computations on a Laminar Airfoil,
Presented at XXV OSTIV Congress, Saint-Auban, France, 1997, 26 p.
(ref. for abstract: Paper 1.1.5, XXV OSTIV CONGRESS 1997, Preprint, Saint Auban sur Durance, France, 3 to 11 July 1997, Text prepared by OSTIV Secreteriate c/o Institut für Physik der Atmosphäre, DLR, D-82232 Wessling, Germany, 25 April 1997.)

Based on reports:

Soinne E., Evaluation of Navier-Stokes program NS2D for a low speed airfoil, Royal Institute of Technology, Department of Aeronautics, Report 97-2, 1997, 53 p.

Soinne E., Analysis of FX 61-163 Airfoil with MSES Program, Royal Institute of Technology, Department of Aeronautics, Report 97-3, 1997, 44 p.

Paper II:
Soinne E., Validation of Navier-Stokes Computations and a Transition Model,
Presented at the XXVI OSTIV Congress, Bayreuth, Germany, August 1999, 10 p.

Based on report:

Soinne E., Validation of Navier-Stokes Computations and a Transition Model, Royal Institute of Technology, Department of Aeronautics, Report 99-15, 1999, 56 p.

Paper III:
Soinne E., CFD Computations on Aircraft Control Surface Flow,
Presented at 11th Nordic Seminar on Computational Mechanics,
Stockholm, Sweden, 1998, 27 p.
(ref. for abstract: Eriksson A., Pacoste C. (editors), Proceedings of the NSCM-11: Nordic Seminar on Computational Mechanics, Royal Institute of Technology, Department of Structural Engineering, TRITA-BKN. Bulletin 39, 1998, ISSN 1103-4270, ISRN KTH/ BKN/B--39--SE, p. 65...68)

Based on Report:

Soinne E., Validation of CFD Computations on Control Surfaces, Royal Institute of Technology, Department of Aeronautics, Report 98-15, 1998, 83 p.

Paper IV:
Soinne E., Aerodynamically Balanced Aileron Design, AIAA Paper 99-3147,
Presented at 17th AIAA Applied Aerodynamics Conference, Norfolk, VA, USA, June-July 1999, 11 p.

Based on Reports:

Soinne E., Literature Review on Aileron Design,
Royal Institute of Technology, Department of Aeronautics,
Skrift 97-17, 1997, 25 p. + Appendices 125 p.

Soinne E., Aerodynamically Balanced Aileron Design, Royal Institute of Technology, Department of Aeronautics, Report 98-37, 1998, 94 p.

Paper V:
Soinne E., Flight Mechanical Design of Aerodynamically Balanced Ailerons, AIAA Paper 2000-3915, Presented at AIAA Atmospheric Flight Mechanics Conference, Denver, CO, USA, August 2000, 11 p.

Based on Reports:

Soinne E., Dimensioning Cases for the Aileron Design of a Commercial Aircraft, Royal Institute of Technology, Department of Aeronautics, Report 97-25, 1997, 37 p.

Soinne E., Flight Mechanical Design of Aerodynamically Balanced Ailerons, Royal Institute of Technology, Department of Aeronautics, Report 99-16, 1999, 145 p.

Paper VI:
Soinne E., Effects of Tolerances on Aerodynamically Balanced Ailerons, AIAA Paper 2001-0424, accepted for presentation at 39th AIAA Aerospace Sciences Meeting and Exhibit, Reno, NV, USA, Jan 2001, 11 p.

Based on Report:

Soinne E., Effects of Tolerances on Aerodynamically Balanced Ailerons, Royal Institute of Technology, Department of Aeronautics, Report 2000-7, 2000, 172 p.

3. TWO-DIMENSIONAL TRAILING EDGE FLOW

3.1 ns2d code

The Saab Navier-Stokes code ns2d solves the two-dimensional time-dependent compressible Reynolds averaged Navier-Stokes equations written in conservative form. The equations are solved in a structured multi block domain. The mean flow equations are discretized in space using a cell-centered finite volume approximation. Central differences are used for the convective fluxes. For the viscous fluxes the gradients of velocity and temperature are evaluated at the cell interfaces using the gradient theorem on auxiliary cells. The viscous fluxes are then computed in the same way as the convective fluxes. A blending of adaptive second and fourth order artificial dissipation terms are added to the numerical scheme to damp spurious oscillations and improve convergence. In the k-ε turbulence models the diffusive terms are discretized using central differences while for the convective terms a hybrid of upwind and central differencing is used. The discretization results in a tridiagonal system of linear algebraic equations which are solved with an ADI method.

The mean flow equations are integrated in time using an explicit five-step Runge-Kutta scheme. Local time steps as well as multigrid technique are available for convergence acceleration. The multigrid technique is based on a Full Approximation Scheme (FAS). The far-field boundary conditions utilize the one-dimensional Riemann invariants combined with a velocity correction based on equivalent circulation Γ. The Airfoil lift, drag and moment coefficients are determined by integration of the airfoil surface pressure p and the wall stress τ_w.

The code has been validated in the BRITE/EURAM EUROVAL and GARTEUR collaboration projects with applications such as the Aerospatiale AS239 airfoil, the NLR7301 flapped airfoil and the Airbus A310 three element airfoil. At Saab the code has been used for example for the wing flap and horizontal tail computations of Saab 2000, for details see ref. 34.

3.1.1 Governing equations

The compressible flow Navier-Stokes equations have the general form, where conservation of mass is written as

$$\frac{\partial}{\partial t}\rho + \frac{\partial}{\partial x_i}(\rho u_i) = 0 \tag{1}$$

where ρ is density, t is time and u_i the velocity component in Cartesian coordinate direction x_i. The transport equation of momentum is written

$$\frac{\partial}{\partial t}(\rho u_i) + \frac{\partial}{\partial x_j}(\rho u_i u_j + p\delta_{ij}) = \frac{\partial \tau_{ij}}{\partial x_j} \tag{2}$$

p is pressure, δ_{ij} Kronecker´s delta and τ_{ij} is the viscous stress tensor defined for a Newtonian fluid by

$$\tau_{ij} = \mu\left(2s_{ij} - \frac{2}{3}\frac{\partial u_m}{\partial x_m}\delta_{ij}\right) \tag{3}$$

where μ is dynamic viscosity and s_{ij} is the strain tensor

$$s_{ij} = \frac{1}{2}\left(\frac{\partial u_i}{\partial x_j} + \frac{\partial u_j}{\partial x_i}\right) \tag{4}$$

The conservation of total energy is written as

$$\frac{\partial}{\partial t}\left[\rho\left(e + \frac{1}{2}u_i u_i\right)\right] + \frac{\partial}{\partial x_j}\left[\rho u_j\left(h + \frac{1}{2}u_i u_i\right)\right] = \frac{\partial}{\partial x_j}(u_i \tau_{ij}) - \frac{\partial q_j}{\partial x_j} \tag{5}$$

where e is specific internal energy, h specific internal enthalpy

$$h = e + p/\rho \tag{6}$$

and q heat flux. In order to close the system of equations relations are needed for pressure, internal energy and temperature. For a caloric perfect gas the thermodynamic relations are

$$e = C_v T \tag{7}$$

$$p = \rho R T \tag{8}$$

where C_v is specific heat in constant volume, R gas constant and T temperature.

3.1.2 Two-dimensional formulation in ns2d

Integrating the two-dimensional unsteady compressible Reynolds averaged Navier-Stokes equations, written in conservative form, over an arbitrary quadrilateral cell $\Omega_{i,j}$ yields following the nomenclature of ns2d (ref. 34)

$$\int\int_{\Omega_{i,j}} \frac{\partial W}{\partial t} dS + \oint_{\partial\Omega_{i,j}} H(W)\hat{n} ds = 0 \tag{9}$$

Here the vector of conserved variables contains the fluxes $W=\{\rho, \rho\overline{u_1}, \rho\overline{u_2}, \rho E\}^T$, where $\overline{u_1}$ and $\overline{u_2}$ are the mean velocity components in Cartesian coordinate directions 1 and 2 and E is the specific total energy

$$E = e + \frac{1}{2}(u_1^2 + u_2^2) \tag{10}$$

The flux tensor H is composed of convective, viscous and turbulent parts

$$H = (F^c - F^v - F^t)e_1 + (G^c - G^v - G^t)e_2 \tag{11}$$

in the coordinate directions 1 and 2 respectively. The convective fluxes are given by

$$F^c = \begin{bmatrix} \rho\overline{u_1} \\ \rho\overline{u_1}^2 + p \\ \rho\overline{u_2 u_1} \\ \rho\overline{u_1}H \end{bmatrix}, \quad G^c = \begin{bmatrix} \rho\overline{u_2} \\ \rho\overline{u_1 u_2} \\ \rho\overline{u_2}^2 + p \\ \rho\overline{u_2}H \end{bmatrix} \tag{12}$$

where H is the stagnation enthalpy

$$H = E + p/\rho \tag{13}$$

The viscous and turbulent fluxes are given by

$$F^v + F^t = \begin{bmatrix} 0 \\ \tau_{11} - \rho\overline{u_1'^2} \\ \tau_{21} - \rho\overline{u_2' u_1'} \\ \overline{u_1}(\tau_{11} - \rho\overline{u_1'^2}) + \overline{u_2}(\tau_{12} - \rho\overline{u_1' u_2'}) - q_1 \end{bmatrix} \tag{14}$$

$$G^v + G^t = \begin{bmatrix} 0 \\ \tau_{12} - \rho\overline{u_1' u_2'} \\ \tau_{22} - \rho\overline{u_2'^2} \\ \overline{u_1}(\tau_{21} - \rho\overline{u_2' u_1'}) + \overline{u_2}(\tau_{22} - \rho\overline{u_2'^2}) - q_2 \end{bmatrix} \tag{15}$$

An overbar denotes timeaveraged mean value and an apostrophe a fluctuation. Using Fourier´s law and an a closure approximation for the turbulent part the heat-flux can be expressed as

$$q_i = -C_p\left(\frac{\mu}{Pr} + \frac{\mu_T}{Pr_T}\right)\frac{\partial T}{\partial x_i} \qquad i = 1,2 \tag{16}$$

where Pr is Prandtl number, Pr_T Prandtl number for turbulent flow and μ_t turbulent eddy viscosity. For a Newtonian fluid the stress tensor τ_{ij} can be expressed in terms of the mean velocity gradients and the dynamic viscosity μ as

$$\tau_{ij} = \mu\left(\frac{\partial \overline{u_i}}{\partial x_j} + \frac{\partial \overline{u_j}}{\partial x_i} - \frac{2}{3}\frac{\partial \overline{u_m}}{\partial x_m}\delta_{ij}\right) \qquad i,j = 1,2 \qquad (17)$$

The remaining unknown terms in the system of equations are the Reynolds stresses $-\rho\overline{u'_i u'_j}$. Applying the Boussinesq eddy viscosity concept the Reynolds stresses can be expressed as

$$\rho\overline{u'_i u'_j} = \mu_T\left(\frac{\partial \overline{u_i}}{\partial x_j} + \frac{\partial \overline{u_j}}{\partial x_i} - \frac{2}{3}\frac{\partial \overline{u_m}}{\partial x_m}\delta_{ij}\right) - \frac{2}{3}\delta_{ij}\rho k \qquad i,j = 1,2 \qquad (18)$$

where k is turbulent kinetic energy.

Using spatial discretization and numerical integration in time a stationary solution is sought for the vector of conserved variables W that satisfies the Navier-Stokes equations in the entire flow field. In two-dimensional flow there are four unknown flux variables in every point. The value of turbulent eddy viscosity μ_t needed in every point is solved through the turbulence model which introduces up to two additional unknowns. It is worth while noticing that the elements in the system matrix are dependent on Mach and Reynolds numbers.

3.1.3 Turbulence models

Turbulence models are needed for the closure of Navier-Stokes equations because Direct Numerical Simulation is not possible in the computation of practical real cases due to excessive computing times. In algebraic turbulence models no differential equations are needed but turbulent eddy viscosity is computed from the main flow through a set of algebraic equations. The turbulence models based on two differential equations are called two-equation models. The k-ε turbulence models employed in this investigation belong to this category. In these models the turbulent kinetic energy k and its dissipation rate ε are obtained from their transport equations that have a generalized form

$$\frac{\partial}{\partial t}(\rho k) + \frac{\partial}{\partial x_j}(\rho \overline{u_j} k) = \frac{\partial}{\partial x_j}\left[\left(\mu + \frac{\mu_T}{\sigma_k}\right)\frac{\partial k}{\partial x_j}\right] + P_k - \rho\varepsilon - S_k \qquad (19)$$

$$\frac{\partial}{\partial t}(\rho \varepsilon) + \frac{\partial}{\partial x_j}(\rho \overline{u_j} \varepsilon) = \frac{\partial}{\partial x_j}\left[\left(\mu + \frac{\mu_T}{\sigma_\varepsilon}\right)\frac{\partial \varepsilon}{\partial x_j}\right] + \frac{\varepsilon}{k}(c_{\varepsilon 1} f_1 P_k - c_{\varepsilon 2} f_2 \rho\varepsilon) - S_\varepsilon \qquad (20)$$

where P denotes a production term and S a source term. Factors f are damping functions in the vicinity of a wall and c_ε are empirical constants. Depending on the turbulence model in question some terms may be omitted in the transport equations. Kinetic energy and its dissipation rate can be solved for using equations (19) and (20) and the associated turbulent eddy viscosity is obtained from the equations applicable for the turbulence model. In this work two k-ε turbulence models have been utilized: a two-layer model, based on Jones-Launder k-ε model with a Wolfshtein one equation model adopted near the walls, and a modification of the two-layer model with an eddy viscosity limiter (Shear Stress Transport SST). The employed turbulence models are documented in paper I.

3.1.4 Transition model

Transition is predicted by computing the laminar boundary layer parameters with Thwaites´ method and checking transition due to Tollmien-Schlichting instability waves with the e^N-method. Thwaites´ method also gives the separation point for the laminar boundary layer. The determination of the transition location is an iterative process in the code.

In Thwaites´ method algebraic relations are obtained from assumptions of uni-parametric velocity profiles between boundary layer momentum thickness θ, shape parameter H and the friction coefficient c_f that are the unknowns in the von Kármán momentum integral equation

$$\frac{d\theta}{ds} + (2 + H)\frac{\theta dU_e}{U_e ds} = \frac{1}{2}c_f \tag{21}$$

where s is the streamwise coordinate and U_e the velocity at the boundary layer external edge. By introducing a dimensionless pressure gradient parameter

$$\lambda = \frac{\rho\theta^2}{\mu}\frac{dU_e}{ds} \tag{22}$$

and applying Thwaites´ approximation for the right hand side of the rewritten integral equation a first order differential equation is obtained for the momentum thickness (see Moran, ref. 44)

$$\frac{d}{ds}(\theta^2 U_e^6) = 0.45\nu U_e^5 \tag{23}$$

where ν is kinematic viscosity.

The velocity of an inviscid flow at stagnation point is generally analytic and can be expanded in a power series at that point. Substituting a linear approximation for the velocity into equation (23), integrating and assuming that the momentum thickness is finite at the stagnation point an expression for it is obtained. The momentum thickness can then be integrated downstream the boundary layer using equation (23). The form parameter is computed as function of λ using the correlation formulas given by Cebeci and Bradshaw in ref. 8. If separation of the laminar boundary layer occurs before the transition, it is assumed in the code that transition takes place 2% chord downstream of the separation point.

The transition prediction, based on linear stability theory, assumes that transition will occur when the most amplified Tollmien-Schlichting waves have grown a factor e^N. Drela and Giles (ref. 17) solved the Orr-Sommerfeld equation using Falkner-Skan velocity profiles for the spatial amplification rates in a range of shape parameters and unstable frequencies. The logarithm of the amplification ratio N is calculated by integrating the local amplification rate downstream from the stagnation point

$$N = \int_{Re_{\theta c}}^{Re_\theta} \frac{dN}{dRe_\theta} dRe_\theta \tag{24}$$

No amplification will take place for $Re_\theta < Re_{\theta c}$ by setting $dN/dRe_\theta = 0$. The slope of the maximum amplification rate dN/dRe_θ is assumed to be only a function of the local shape factor H using an empirical relation and the critical Reynolds number $Re_{\theta c}$ is also expressed through an empirical formula (see ref. 17). Transition occurs when N reaches some critical value. Throughout this work the default value $N_{crit}=9$ has been used.

The self-similar Falkner-Skan velocity profiles, on which the method is based, are not exactly valid for airfoil boundary layers in general. However, according to Dini et al (ref. 15) the shape factor distribution characteristics of most airfoil flows are smooth enough and the envelope method of Drela and Giles is sufficiently accurate before laminar separation.

3.2 FX 61-163 airfoil

3.2.1 Airfoil data

FX 61-163 is a classical laminar airfoil that has been tested in the laminar flow wind tunnel at the Technical University of Stuttgart (ref. 1), at the Technical University of Delft (ref. 6) and at the University of Alberta (ref. 38). The quality of the flow in the different tunnels, the measuring techniques and the accuracy of the wind tunnel models are reviewed in paper I. The measurements are consistent on lift and drag coefficient, but on pitching moment the results obtained in Delft somewhat deviate from those of the other two. This is believed to be a result from the finite trailing edge thickness and slightly higher thickness ratio of the experimental model. The conclusion is that the measurements are reliable and support each other. The weak point in the experiments is the model geometry that in the Delft model was slightly different from the nominal airfoil. The deviation in the Stuttgart model was smaller but the exact test geometry was not reported.

The mesh for the computations was created with an in-house program at Saab. The created C-mesh has 64 cells perpendicular and 256 cells parallel to the airfoil surface. The airfoil trailing edge ends in a single point thus having zero thickness as shown in the grid in fig. 2. To guarantee a sufficient resolution in the viscous sublayer the grid was generated so that the distance from the airfoil contour should satisfy the condition $y^+ \leq 1$ at the first cell centre. This gave a first cell height in the order of 10^{-5}c.

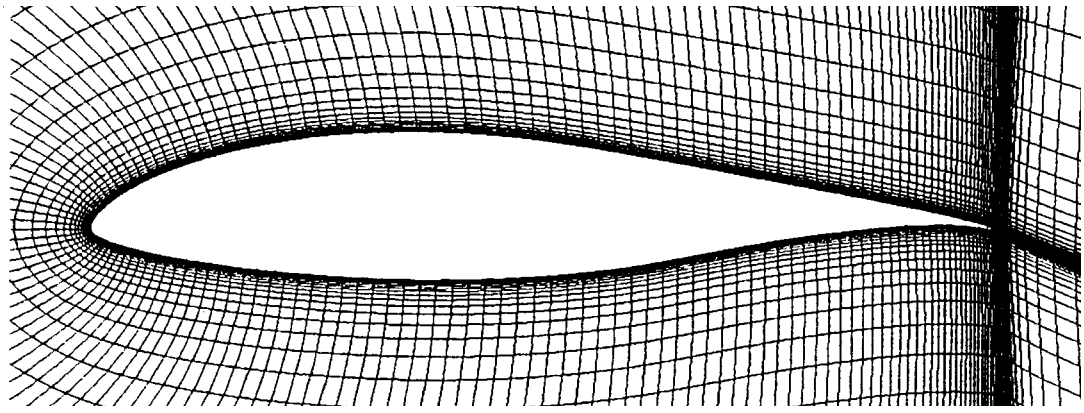

Figure 2. A close-up view of the mesh used on FX 61-163 airfoil (ref. 58).

3.2.2 ns2d results

Four sets of computations were performed in this study. Transition free computations were made at Reynolds number $1.5 \cdot 10^6$ and at Mach number 0.1 with the two-layer turbulence model and the modified turbulence model. The transition locations for the smooth airfoil were taken from the wind tunnel measurements of ref. 1, because at the time of the computations there was no transition model available in the code. Transition fixed computations were made with the two-layer model at Reynolds numbers $1.0 \cdot 10^6$ and $2.5 \cdot 10^6$.

The computations were made on a SGI Indigo R4000 workstation with a 32Mb RAM using the version of the ns2d code labeled NS2D. The two-layer k-ε turbulence model was utilized for the computations and a modification of it with an eddy viscosity limiter (Shear Stress Transport SST) was employed to study the airfoil stall. The number of work units (iterations on the fine mesh level) was selected as 9000 which gave a run time of 13.5 hours with the two-layer model. Convergence was controlled by monitoring the rms value of the density residual and pressure lift coefficient c_{Lp}. With the modified SST turbulence model the iterations were continued until the change in lift coefficient was less than 1% of its value. This showed to require a number of iterations up to 54000 work units.

The smooth airfoil polar was computed using the two-layer turbulence model at Reynolds number $1.5 \cdot 10^6$. As shown in fig. 7 in paper I the lift curve slope was approximately 5% higher than the measured reference curve. In the computed values there was also a shift of roughly 0.5^o in the zero lift direction. Consequently the computed lift coefficient values were around 0.08 higher than the measured ones in the linear lift range. The computations with transition fixed showed that the lift curves were lowered due to a thicker boundary layer, see figures 8 and 9 in paper I. However the curves were still above the measured ones in the same way as for the smooth airfoil.

The moment coefficients for the smooth airfoil at Reynolds number $1.5 \cdot 10^6$, computed with the basic two-layer turbulence model, are depicted in figure 7 of paper I. For smooth airfoil the computed moment coefficient curve showed a similar form as measured in Stuttgart. The absolute values were somewhat higher, $\Delta c_{m.25}=0.02$, which is roughly 20% of the measured value. It is logical that, with computed lift coefficients exceeding the measured values, the computed moment coefficients show more negative values than the measured ones, if the deviation is due to the flow conditions mainly at the airfoil trailing edge. The moment coefficients for the airfoil with transition fixed at Reynolds number $2.5 \cdot 10^6$ showed only small differences compared with the transition free case. The numerical results on the aerodynamic coefficients are found in ref. 58.

When using the modified turbulence model it was not sufficient to check the density residual when monitoring the convergence but lift coefficient changed slowly even if no change was noticed on the density residual.

The performed runs with the Navier-Stokes code ns2d show that computation of a complete airfoil polar is needed for insight into the overall performance of the program.

3.2.3 MSES results

Because the lift curve computed with ns2d deviated from the wind tunnel measurements more than expected calculations with MSES code were made for comparison (ref. 55). MSES is a computer program, developed at MIT by Drela (ref. 16), for the analysis and design of two-dimensional transonic airfoils and cascades. It uses Newton method to solve the Euler equations on an intrinsic streamline grid coupled with an integral boundary layer method. A detailed description of the theory included into the program is presented in ref. 18.

Three sets of calculations were performed at $Re=1.5 \cdot 10^6$:
- FX 61-163 nominal airfoil
- FX 61-163 with trailing edge thickened to 0.2% of chord
- FX 61-163 with trailing edge clipped to a thickness of 0.22% of chord

The three trailing edge geometries are shown in figure 3.

The lift and pitching moment curves of the nominal airfoil, computed with MSES and ns2d, were virtually the same in the linear lift range, see fig. 18 of paper I. The thickening of the airfoil trailing edge had only a marginal effect on the lift curve and moment coefficient. The clipped trailing edge produced considerably less lift and pitching moment.

The chosen FX 61-163 airfoil is a demanding test case. The computations on the trailing edge modifications show that even small changes at a strongly cusped trailing edge have a significant effect on the lift and pitching moment coefficients. This may be a major explanation for the differences in the computed and measured results as the true trailing edge geometry of the wind tunnel models is not known. Detailed studies with the exact model geometry and refined grids should be carried out to confirm the differences.

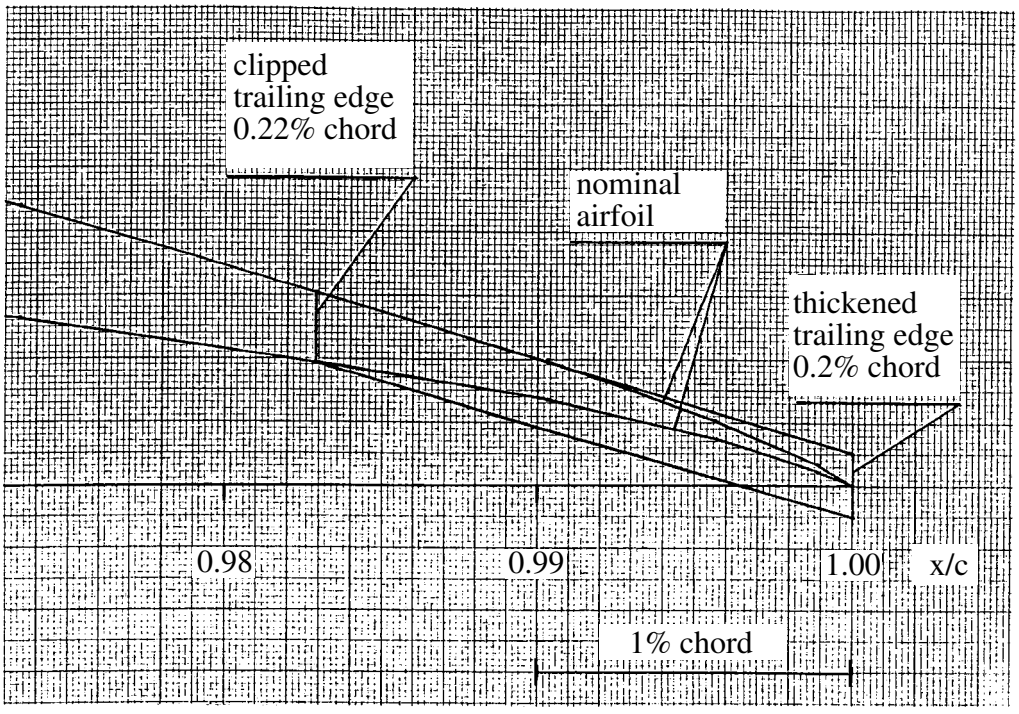

Figure 3. Close-up view of the trailing edge modifications of FX 61-163 airfoil (ref. 55).

3.3 FX 66-17AII-182 airfoil

3.3.1 Airfoil data

FX 66-17AII-182 airfoil was chosen because wind tunnel tests, performed in NASA low-turbulence pressure tunnel in Langley by Somers (ref. 63), were available with a measurement of the actual model geometry. The wind tunnel model had a finite thickness trailing edge of 0.08 percent of the airfoil chord. In the computations of slotted airfoils of refs. 2 and 12 as an example the main airfoil blunt trailing edge was modified to end in zero thickness to ease the meshing and the computations. However, the effect of a geometry modification on the computed results may always be questioned. To avoid that kind of discussion the grid generation was here performed on the exact wind tunnel model geometry. The airfoil contour is shown in fig. 4.

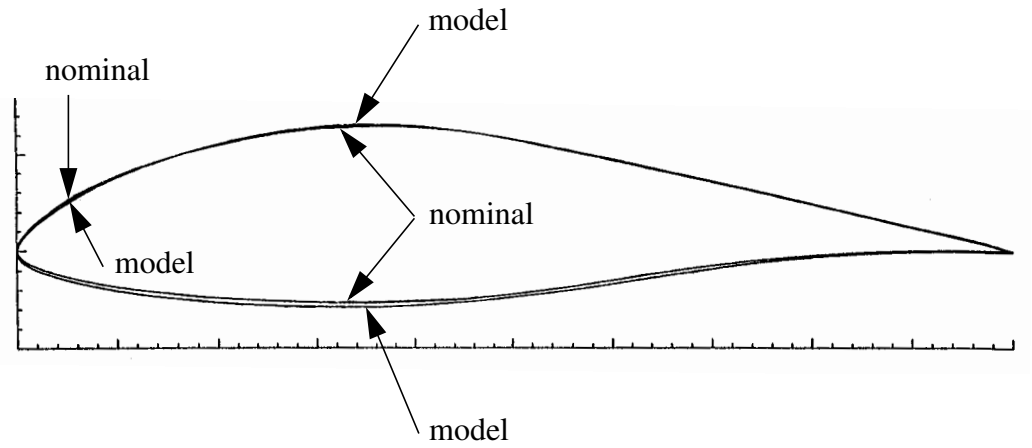

Figure 4. Contours of FX 66-17AII-182 nominal airfoil and wind tunnel model (ref. 63).

3.3.2 Grid generation

The modified C-type mesh was extended 10 chord lengths away from the airfoil. The four block mesh, contained altogether 30700 nodes. The number and distribution of nodes and stretching of cells were based on the grid variation and grid convergence studies performed in ref. 61. The geometry of the airfoil blunt trailing edge was accurately modeled by using 32 cells over the trailing edge thickness, see fig. 5.

To ensure a sufficient resolution of the boundary layers the first cell size was based on the requirement of $y^+=1$ at the cell center. Using the 1/7 power velocity profile approximation for incompressible flow turbulent boundary layer over a flat plate (ref. 52) an analytic expression was derived for the required cell size ds divided by the airfoil chord c

$$\frac{ds}{c} = 2\sqrt{\frac{0.37^{1/4}\left(\frac{x}{c}\right)^{1/5}}{0.0225\mathrm{Re}^{9/5}}} \tag{25}$$

The expression for the values at the trailing edge (x/c=1) is depicted in fig. 6. The incompressible flow assumption gives a slightly conservative estimate for the required cell size

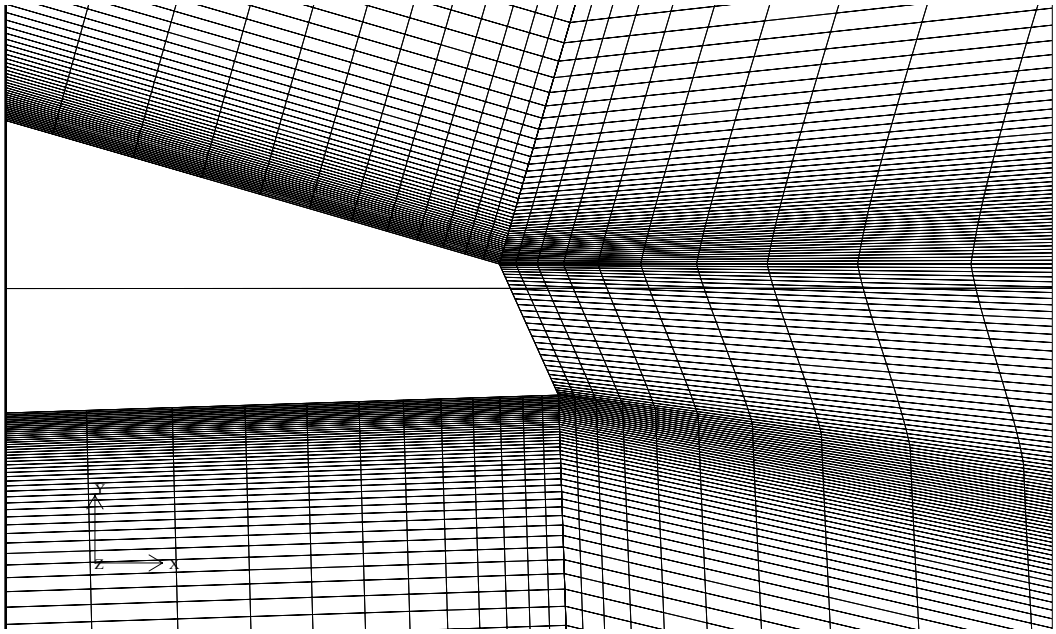

igure 5. Close-up view of the grid at the 0.08% chord thick trailing edge of FX 66-17AII-182 airfoil (ref. 62).

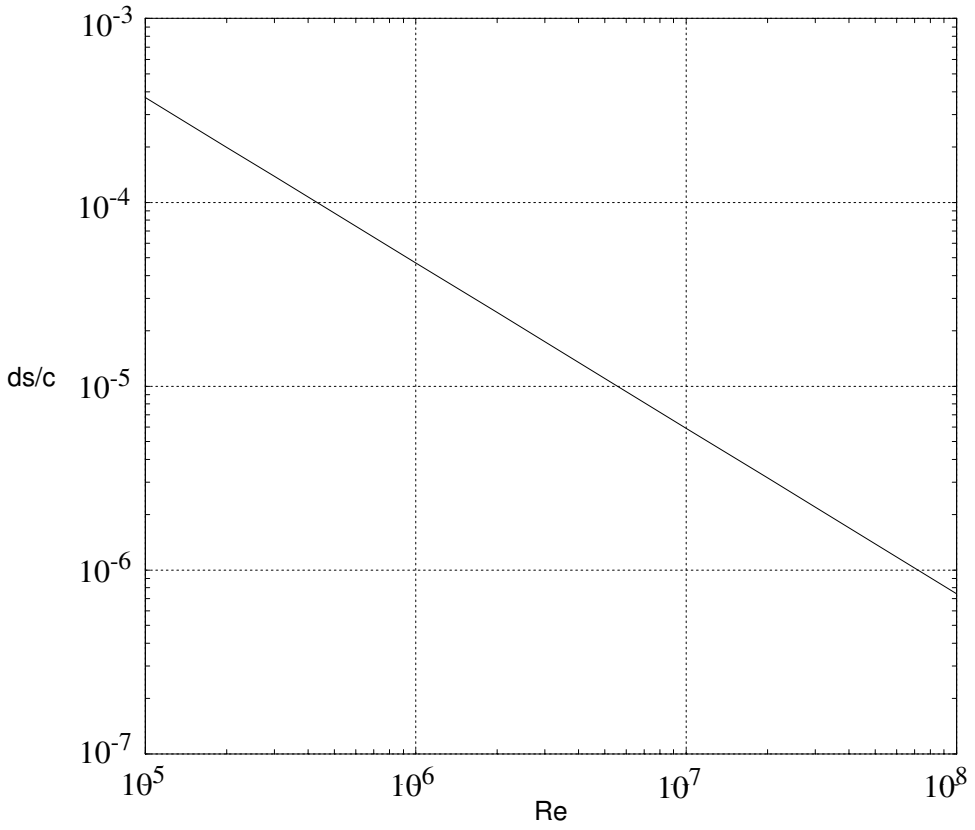

Figure 6. Maximum first cell size divided by airfoil chord as function of Reynolds number based on the requirement $y^+=1$ at the first cell center at airfoil trailing edge (ref. 54).

in subsonic flow, because the boundary layer thickness increases with Mach number due to the increase in temperature of the air near the wall. Grid resolution requirements are much more demanding for turbulent than for laminar boundary layers (ref. 49), which can be explained by the fact that the form of the boundary layer velocity profile in a laminar boundary layer is linear in a proportionally larger part of the layer thickness. A physical explanation, based on capturing the linearity of the viscous sublayer, was given in paper III on the requirement of $y^+=1$ at the first cell center.

3.3.3 ns2d results

In this study (ref. 62) three sets of computations were carried out. In the computations transition was specified according to the wind tunnel measurements at $Re=1.5\cdot10^6$ and Ma=0.10. Computations were also made with the transition model at $Re=1.5\cdot10^6$ and $Re=3.0\cdot10^6$ at the same Mach number. In this work the two-layer turbulence model was used with an automatic routine for switching between the inner and outer models.

A special version of the code ns2dr8_trans, based on ns2d version 1.36, was used with the two-layer turbulence model together with an automatic routine for switching between the inner and outer models. With a 194 MHz SGI Power Challenge processor the computing time to 20000 work units was approximately 12 hours. Convergence was ensured by monitoring the rms values of the time derivatives of the density and turbulent kinetic energy residuals as well as the aerodynamic coefficients on lift, drag and pitching moment.

Complete polars were computed in the three cases with the results collected into figs. 7 and 8 of paper II. The transition model made it possible to make computations with experimental cases where transition locations where not measured. At $Re=1.5\cdot10^6$ the computed transition locations were close to the experimental values. The computed drag polars reproduced the experimental drag values fairly well at both Reynolds numbers. The matching of the computed and measured lift and pitching moment curves was excellent in the linear lift range, showing that an exact modeling of the airfoil contour at the trailing edge is essential.

4. TWO-DIMENSIONAL FLOW AROUND AILERONS

4.1 NSMB code

NSMB is a three-dimensional multi block Navier-Stokes solver developed by two universities, EPFL in Switzerland and KTH in Sweden, a research institute CERFACS in France and two aircraft industries, Aerospatiale Avions in France and Saab Aerospace in Sweden.

NSMB offers possibilities for both steady and unsteady computations, different discretization schemes and an explicit and implicit solver. In the present investigation all computations were steady using the 2D option of the code. For spatial discretization Roe´s upwind scheme was used in which artificial viscosity is implicitly included. The scheme is a Total Variation Diminishing (TVD) version of Roe´s scheme applying the Monotone Upwind Schemes for Conservation Laws (MUSCL) extrapolation. The gradient theorem is used to determine the viscous fluxes.

The Lower-Upper Symmetric Gauss-Seidel (LU-SGS) implicit solver with matrix approximation was used for the time integration. Multigrid technique was not used in the computations. Characteristic variables, which is basically a linearized form of Riemann invariants, was chosen as the far-field boundary condition. Far-field vortex correction on velocities was not used. Aerodynamic coefficients were determined through surface integration.

Two algebraic turbulence models, Baldwin-Lomax and Granville, and one two-equation turbulence model, Chien´s k-ε model, were used in this study. The turbulence models are documented in the program User´s manual in ref. 66.

4.2 MS(1)-0313 airfoil

4.2.1 Airfoil data

The MS(1)-0313 is a 13% thick medium speed airfoil designed at NASA for turbulent flow at medium subsonic Mach numbers. For practical reasons the trailing edge thickness is finite being 0.66% chord. The airfoil has been tested in the wind tunnel at Wichita State University with a 20% chord plain aileron with a 0.5% chord slot between the aileron and the main wing (ref. 69). The tests were performed at a low Mach number of 0.13 and Reynolds number of $2.2 \cdot 10^6$. Transition was fixed on the airfoil upper surface at 5% chord and on the lower surface at 10% chord. Standard wind tunnel corrections were applied on the measured values. The tests with the basic airfoil (slot closed) match well the results of the previous NASA wind tunnel experiments (ref. 41).

The thickness of the MS-series airfoils used on Saab 2000 wing varies with an increasing thickness towards the wing root. The ailerons on Saab 2000 are aerodynamically balanced so the geometry of the test section aileron is quite different, however there is a slot between the aileron and wing, see fig. 7.

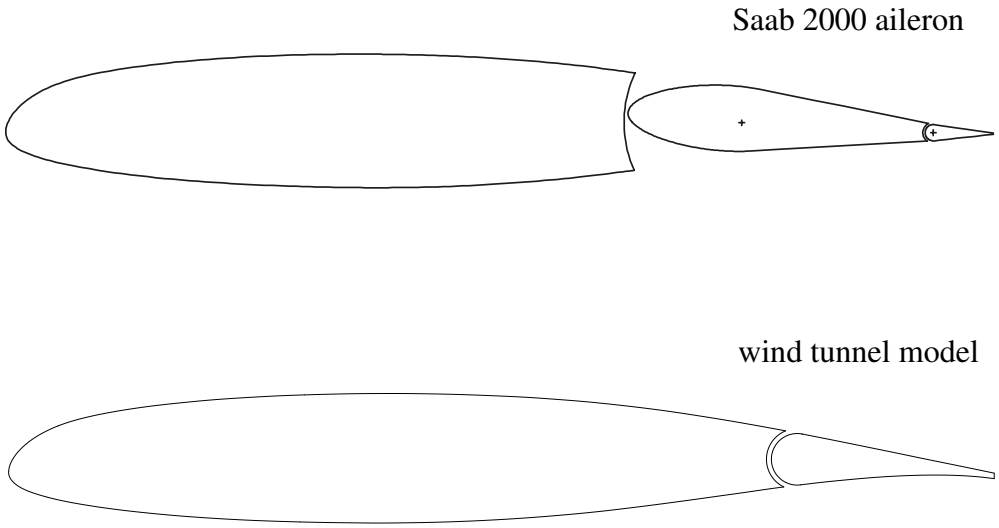

igure 7. Contours of MS-series airfoils as used on Saab 2000 and in the wind tunnel test (refs. 61, 69).

4.2.2 Grid generation

Grids were created at aileron deflections 10^o, 0^o and -10^o. The created grids were of modified C-type with one type C grid enclosing the aileron and passing through the slot and another one enclosing the airfoil and the first mentioned grid. The mesh was extended 10 chord lengths away from the airfoil to ensure reasonable farfield boundary conditions. Sufficient boundary layer resolution was ensured by basing the first cell size on the curve of fig. 6. The streamwise cell size at the trailing edge and the stretching values were carefully chosen to ensure sufficient resolution. Again the airfoil trailing edge was modeled accurately avoiding simplifications. 64 cells were chosen over the trailing edge thickness and across the aileron slot. This gave around 62000 nodes for the two-dimensional ns2d grids and 187000 for the three-dimensional grids of NSMB.

The meshes were visually checked by plotting the maximum angle deviation, see example in fig. 8. The maximum distortion appears in the area where the cells emanating from the aileron slot meet the cells in the upper and lower boundary layers. This is inevitable with a structured mesh and the distortion is limited to local small areas. The mesh is so dense in these areas that no anomalies were noticed in the solutions.

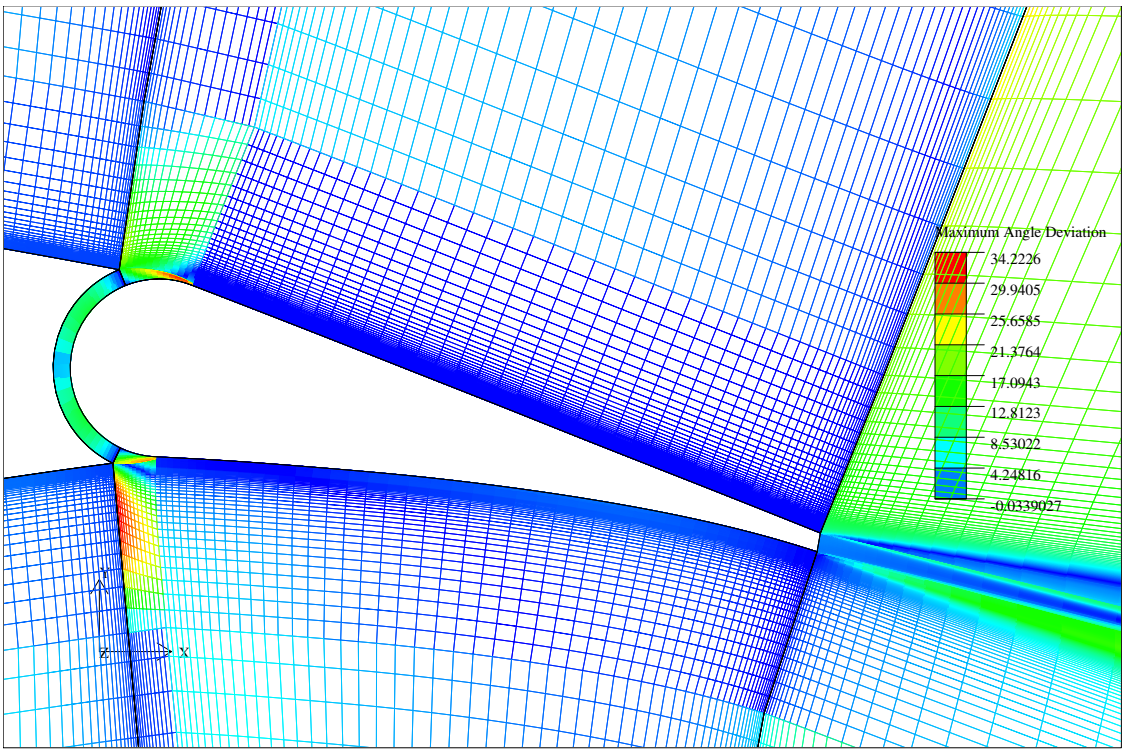

Figure 8. Maximum angle deviation around the aileron of MS(1)-0313 airfoil with 10^{o} aileron deflection (ref. 61).

4.2.3 Results

The computations were made at an angle of attack in the linear lift range representative for the conditions in approach flight with 5% descent gradient at reference speed V_{REF}.

The main alternative for the computations with ns2d (version 1.36) was the two-layer turbulence model. Some computations were also made with Baldwin-Lomax and Launder-Sharma turbulence models for comparisons. ns2d computations were performed on Cray C90 vector computer having six processors and a theoretical maximum performance of 5.7 Gflops. Convergence was monitored on the rms value of the derivatives of the density and turbulent kinetic energy residuals as well as the aerodynamic coefficients of lift, drag and pitching and hinge moment. Convergence of hinge moment normally required from 50000 to 100000 work units whereas the residuals were not a good indicator of convergence.

Computations with NSMB were performed using the Baldwin-Lomax turbulence model and k-ε turbulence model of Chien. NSMB computations were run on Cray T3E using version 4.21 (February 3rd 1998) on 16 processors. Convergence was monitored on the residuals and the aerodynamic coefficients of lift, drag and pitching moment. The residuals were not a good indicator on convergence.

A summary of the computed results on MS(1)-0313 airfoil with the basic set of grids is shown in table 1 of paper III. In the low speed test case at Ma=0.13 and $Re=2.2\cdot10^{6}$ on

the MS(1)-0313 airfoil the results were practically the same with ns2d and NSMB codes. The computed lift coefficient values agreed well with the measurements only in the case of the negative aileron deflection of -10^o (trailing edge up). The higher the lift coefficient was the larger was the difference between the computed and measured values. The smallest difference in c_L was 0.016 and the largest 0.138, typically below 0.1. A possible explanation for the largest difference at positive aileron deflection may be the fact that k-ε turbulence models are known to predict a too late separation on flows with adverse pressure gradients. Flow visualization showed that there was a separation bubble on the aileron upper surface in front of the trailing edge.

Computations in the original report (ref. 61) were also performed with the slot blocked, see paper IV. According to the computations the reduction in lift coefficient due to the opening of the slot was 0.032 at zero aileron deflection. This agrees fairly well with the reduction of 0.05 in the wind tunnel tests.

The aileron efficiency derivative $\partial c_L/\partial \delta_a$ values were overpredicted roughly by 15%. The ratio of the derivatives for positive and negative aileron deflections was, derived from the computations, 0.70 and from the measurements 0.723. Hence the computations could reproduce the asymmetry in the aileron efficiency in positive and negative deflections, which is due to the aft loading of the basic airfoil.

The hinge moments showed the best results with zero deflection of the aileron, where the difference from the measured values was, say 0.02 (absolute value). At aileron deflection $\pm 10^o$ the difference was approximately 0.05. The computed hinge moment coefficient seemed to be more positive than the measured values.

The obtained accuracy in lift and hinge moment coefficient on MS(1)-0313 airfoil with aileron deflection $\delta_a=10^o$ was less than was hoped for. However, the test case is a modern cambered and rear loaded airfoil. Due to airworthiness requirements on failure cases it is difficult to utilize full cambering in an aileron section of a transport category airplane. This means that on a practical aileron at 10^o deflection a higher computational accuracy can be expected. Another factor contributing to better results in approach flight condition is the clearly higher Reynolds number than in the low speed wind tunnel tests.

4.3 Grid variation

Grid variation studies were undertaken on MS(1)-0313 airfoil with aileron deflection $\delta_a=10^o$ in the low speed test case with ns2d code by

- refining the grid locally in the vicinity of the trailing edge and slot opening
- relaxing the first cell size
- increasing the computational domain size

Local streamwise grid refinement in the vicinity of the trailing edge and the slot opening, where separation bubbles appeared, showed no improvement compared with the basic grid. This was also the case with streamwise grid refinement in the vicinity of the Saab 2000 aileron stagnation point (ref. 70).

First cell size was also relaxed from the conservatively chosen value of the basic grid, corresponding roughly to y^+=0.5, to more closely fulfill the $y^+ \leq 1$ requirement. This relaxation showed no noticeable degradation of the results.

The mesh size was increased from the normal with external boundary at 10 chord lengths from the airfoil to 20 chord lengths. There was practically no change in the aerodynamic coefficients, which is attributed to the applied farfield velocity correction based on an equivalent vortex strength.

4.4 Grid convergence

Grid convergence was studied with the help of the basic mesh that was created with multiples of 4 cells in every subface giving three grid levels denoted as coarse, medium and fine mesh levels. A very fine mesh was created separately by once more doubling the number of cells in the two directions. The number of nodes was altogether 250000. Because obtaining complete grid convergence, i.e. no change of results due to grid refinement, is not possible due to practical limitations on computer resources, the results at infinitely dense grid were estimated with Richardson´s extrapolation.

The convergence on this mesh was slightly worse than on the corresponding basic mesh. The computed results at different grid levels are displayed in fig. 9 as function of grid level parameter n_g. The parameter is proportional to the number of cells in one coordinate direction. The results on coarse mesh level are at $1/n_g$=1 and on very fine mesh level at $1/n_g$=1/8. The scales in the figure have been blown up for presentation.

On lift coefficient the mesh level had a negligible effect on the results, but the computed results did not converge towards the wind tunnel measurements. The fine mesh value exceeded by 0.138 the wind tunnel test result of 1.03.

The hinge moment coefficient converged also quite well with the fine mesh absolute value being only 0.0002 above the infinite mesh result. However, the computed results did not converge towards the wind tunnel measurements. The fine mesh value fell by 0.051 short of the wind tunnel test result of -0.29.

The drag coefficient converged towards the experimental value with the fine mesh value already being within 3%. The medium and coarse level grids were too coarse for the determination of the airfoil drag. The grid convergence on the pitching moment coefficient was good but the fine mesh value differed slightly from the wind tunnel test value.

It is obvious that the discrepancy between the measurements and the fine mesh level values is not due to changes in grid convergence. The fine mesh results are so close to the infinite mesh values that the fine mesh solution is a good engineering approximation. The discrepancies are probably due to the inherent properties of the turbulence model used.

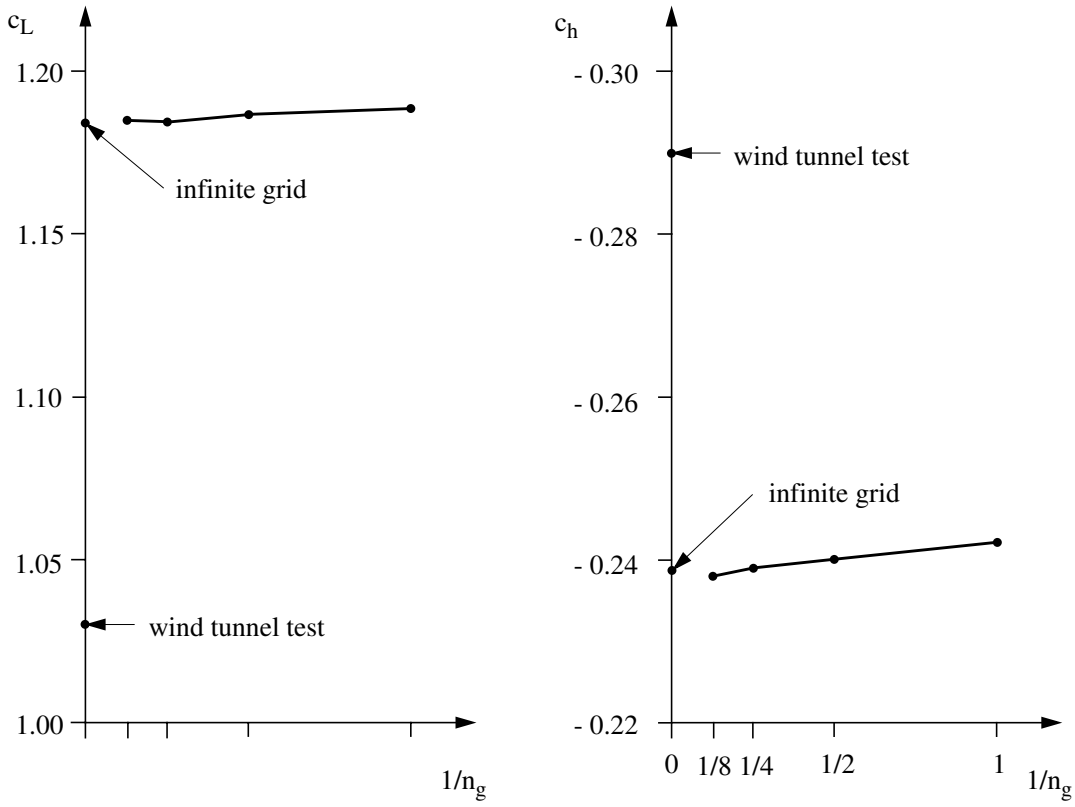

Figure 9. Grid convergence of lift and hinge moment coefficients for MS(1)-0313 airfoil at 10^o aileron deflection and $\alpha=4^o$, Ma=0.13, $Re=2.2\cdot10^6$. Two-layer turbulence model (ref. 61).

4.5 DLBA032 airfoil

4.5.1 Airfoil data

The McDonnel Douglas airfoil DLBA032 with a 25% chord plain aileron is 12.3% thick and designed for supercritical flow and rear loading (ref. 10). The trailing edge thickness is 0.5% chord, see fig. 10. The wind tunnel model was equipped with an adjustable aileron fixed with brackets to the chosen deflection. There was a garage type slot on the upper side between the aileron and main wing. The slot was closed on the lower side thus not permitting any flow between the aileron and main wing.

Wind tunnel measurements were performed in the IAR 1.5m x 0.38m Trisonic Blowdown Wind Tunnel of National Research Council of Canada. The flow quality, measuring techniques and accuracy of the wind tunnel model are reviewed in ref. 61. The purpose of the experiments was to provide an experimental test case for the validation of CFD computations and everything was documented in a detailed way.

The modified C grids were created in the same way as for the MS(1)-0313 airfoil. The garage type slot, going halfway through the wind tunnel model between the aileron and

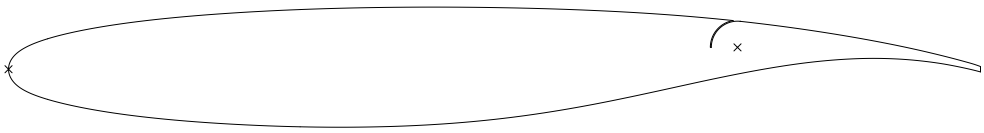

Figure 10. Contour of DLBA032 airfoil wind tunnel model (ref. 10).

the main airfoil, was modeled accurately to give the correct boundary condition at the slot opening. The number of nodes was 53000 for the two-dimensional ns2d mesh and 163000 for the three-dimensional NSMB grid.

4.5.2 Results

For the DLBA032 airfoil the high speed test case was chosen so as to match the local lift at the aileron of Saab 2000 at maximum operating speed V_{MO}/M_{MO}.

Computations were made with the same versions of ns2d and NSMB codes as for the MS(1)-0313 airfoil using the same turbulence models and computers. On normalized total temperature distributions NSMB showed odd looking protuberances emanating from the aileron surface and ns2d showed a slight variation at the shock wave and boundary layers. The distribution obtained with ns2d looked physically reasonable as it was shown (ref. 54) that in viscous compressible flow the total temperature is not exactly constant in the presence of strong heat gradients.

The results in table 2 of paper III show that it was difficult to reach convergence in the computations with a locally transonic flow. The two-layer turbulence model of ns2d predicted the shock wave on the aileron upper surface slightly too far aft. Baldwin-Lomax turbulence model of NSMB gave a fairly accurate solution and reproduced better the suction peak on aileron upper surface aft of the slot. A contributing factor to this was the modeling of the garage type slot between the aileron and main wing to reproduce accurately the wind tunnel model geometry.

5. AERODYNAMIC DESIGN OF AILERONS

5.1 Practical design considerations

5.1.1 Design requirements

For flight safety reasons airworthiness regulations set minimum requirements for the handling qualities of commercial aircraft. In Europe there are joint requirements given by the Joint Airworthiness Authorities JAA (ref. 32) and in the United States there are federal regulations published (ref. 26) by the Federal Aviation Agency FAA. The requirements are continually developed to increase flight safety. However, when applying for the certification of a new airplane it is agreed upon with the authorities about a certain status of the regulations which the airplane shall meet. In the case of Saab 2000 the certification basis was frozen to a level defined in ref. 25.

The regulations specify however only the minimum acceptable requirements for flying qualities. Optimal values and gradings are found in the standards by Society of Automotive Engineers (ref. 13) and American military specifications, MIL Spec (ref. 43). The background of the MIL Spec is described more in detail in refs. 9 and 42. The standards are based on research work published for example in NASA reports, see for example ref. 11. This reference defines the well-known Cooper-Harper pilot rating scale on handling qualities, shown in fig. 11. Satisfactory values have at least pilot rating 3.5 and minimum acceptable values at least rating 6.5. MIL Spec defines flying quality Levels 1, 2 and 3. At Level 1 the flying qualities are clearly adequate for the mission flight phase. At Level 2 the flying qualities are adequate to accomplish the mission flight phase, but some in-

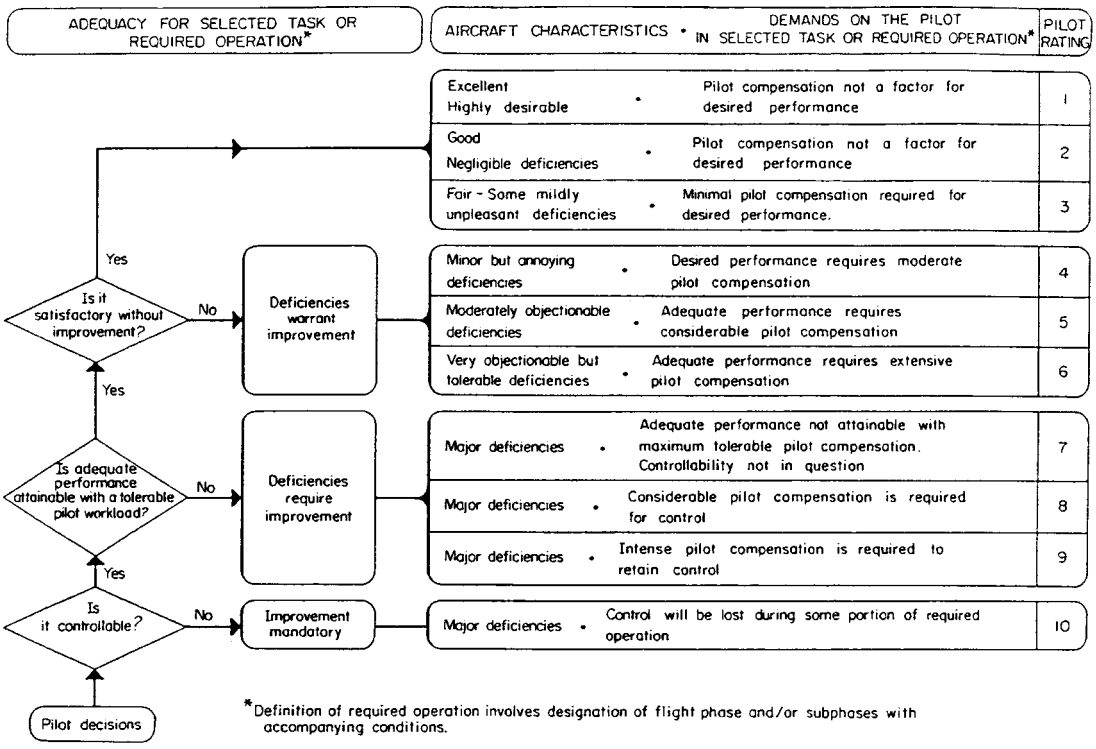

Figure 11. Cooper-Harper handling qualities rating scale (ref. 11).

crease in pilot workload or degradation in mission effectiveness, or both, exists. At Level 3 the airplane can be controlled safely, but pilot work load is excessive or mission effectiveness is inadequate, or both. The Cooper-Harper ratings 3.5 and 6.5 correspond with the lower limit of flying quality Levels 1 and 2, respectively, of the MIL Spec (ref. 9 page 18). The lower limit of Level 3 corresponds with Cooper-Harper rating 9+.

5.1.2 Maximum wheel force

The main target in the design of roll control is to fulfill the requirements on roll efficiency without exceeding the maximum allowable wheel force. Saab 340 was certified in 1984 for a maximum wheel force of 60 lbf but since then the two hand force has been reduced to 50 lbf and one hand operation in approach flight with a maximum 25 lbf wheel force has been introduced in Change 13 of JAR 25 (ref. 32). During the certification of Saab 2000 discussions with the authorities clarified the application of the new requirements. The outcome of the discussions with the certification authorities is summarized in ref. 51 noticing that the approach/landing flare one engine inoperative (OEI) is a one hand case but turbulence is not required to be considered.

A factor further increasing the wheel forces by 10% on Saab 2000 is the reduction of control wheel size by this amount compared with 340. The reason for this was the size and placement of the displays for the electronic flight instrument system (EFIS). The displays were located so low that the wheel size had to be reduced, otherwise the pilots fists would have shadowed the primary flight data display.

Initially an internal specification was written for the handling qualities of Saab 2000 (ref. 33), where a maximum wheel force of 20 lbf was specified, which is even below the 25 lbf limit set by the authorities. In the same specification the maximum control wheel throw was set at 75^{o} whereas a value[1] of 80^{o} is specified in MIL Spec (ref. 43) for a completely mechanical system. It seems that in the internal requirements on aileron dynamics the values were established just by combining the most stringent ones of SAE Standard and MIL Spec independent of flight condition. The design of aerodynamically balanced ailerons is however a demanding task and requires a balanced set of specifications, otherwise problems can arise. After a discussion with the author of the internal specification and the company test pilot the requirements on roll control design were reviewed and a revision was made in ref. 56 to reflect the intention of the airworthiness authorities´ certification requirements (ref. 25) and the additional design targets of the MIL Spec.

5.1.3 Aileron geometry

During the course of the project ailerons were developed in wind tunnel tests with 10 different geometries. The balance ratio varied in the tests between 40 and 50% with a final type design value of 45%. As the wing rear spar location was already fixed when increasing the balance ratio, the aileron hinge line and trailing edge were moved aft, which shows as a notch in the wing trailing edge, see paper IV. The original wing sections and the final aileron contours are shown in fig. 12.

1. The maximum wheel throw is 120^{o} on MD 80 series aircraft with a mechanical control system.

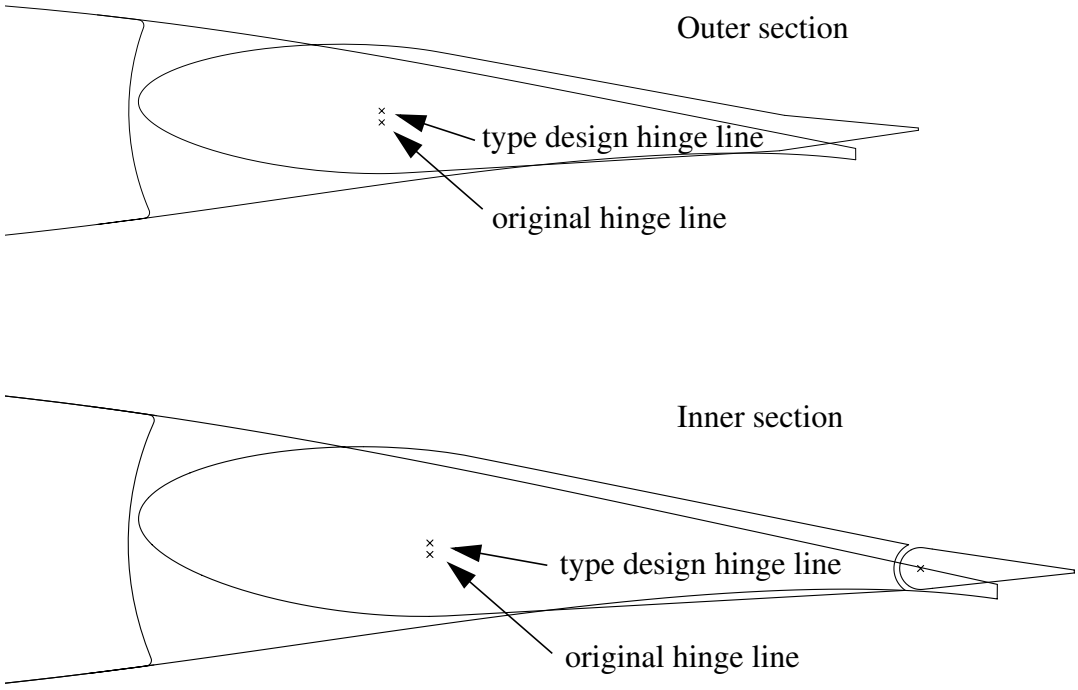

Figure 12. Saab 2000 type design aileron inner and outer sections and the original airfoils (ref. 54).

The tests were performed in a low speed tunnel with a 1:5.7 scaled airplane model. Some high speed tests were performed with smaller complete airplane and half models. One configuration was investigated with different combinations of vortex generators in a transonic tunnel. Aileron tabs were not included in any of the wind tunnel models. However, control surface flow is sensitive for Reynolds number effects and especially the low speed wind tunnel test results were not representative of real flight conditions. Control surface flow is often studied in a pressurized tunnel with a two-dimensional model so that the correct combination of Reynolds and Mach numbers is reached. However, on Saab 2000 no two-dimensional wind tunnel experiments were carried out. Development flight tests with a 2000 geometry aileron on 340 were performed only slightly before the first flight of Saab 2000.

The selected aerodynamic balancing is so high that the absolute value of the hinge moment coefficient derivative $\partial C_h / \partial \delta_a$ is in the order of 0.05 which is clearly below the classical rule of thumb limit of 0.075 (ref. 47). As a consequence production variability on the aileron geometry introduces variation in the hinge moment. Production tolerance requirements were set accordingly.

The nominal size of the gap between the aileron nose and the cove varies from 0.33% chord at the aileron root to 0.48% chord at the aileron tip. A classical rule (ref. 46) says that when the gap size is less than 0.25% chord the gap is effectively sealed and when the gap is larger than 0.5% the gap is effectively fully unsealed. In ESDU (refs. 20 and 21) the maximum limit of gap size has been set at “about 0.2% chord” for a sealed plain control in incompressible two-dimensional flow. In conclusion the chosen gap size may be within a sensitive zone.

5.1.4 Trailing edge reflexion

Control system failures treated in paragraphs 25.671 and 25.673 of the airworthiness regulations for transport category airplane (refs. 26 and 32) state that two-control airplanes must be able to continue safely in flight and landing if any one connecting element in the directional-lateral flight control system fails. An aileron tends to float up when disconnected from the system due to a mechanical failure. The up floating aileron on one side creates a rolling moment that must be compensated. The up-float is even more pronounced with a rear loaded airfoil. Therefore the rear loading was deleted on the Saab 2000 aiöeron.

On Saab 2000 the roll compensation is done by the pilots who can disconnect the left and right ailerons and adjust the other aileron to have the same deflection. The airplane is then in balance for steady level flight. However, there must also be sufficient control authority in the other direction so that the remaining aileron can roll the airplane against the floating one. So the aileron upfloat may not be too large to impair the control authority. On Saab 2000 the consequence has been to deflect the aileron trailing edge and tab upwards so as to reduce the aileron upfloat. Another possibility would be to use a downspring as on Saab 340. The chosen approach has two advantages, namely reduced friction and the ability to handle a failure at any airspeed, as both up-float and tab moment are subject to the same pressure.

The reduced airfoil camber, the slots and the trailing edge reflexion on the aileron affect the wing lift distribution because the local lift coefficients are decreased. Compared with the original airfoil the reduction in lift coefficient is 0.26 at the aileron inner section and 0.32 at the outer section. This manifests as a dip over the aileron in the wing lift distribution as shown in fig. 13, based on extended lifting line computations. The effect of the fuselage and nacelle was ignored in the computations.

The induced drag of the wing was determined using the type design aileron and a wing with the original MS-series airfoil with no local loss of lift over the aileron span and no notch in the trailing edge of the wing planform. The induced drag increase due to the type design aileron was approximately 2% of the airplane total drag in cruise condition with zero angle of attack of the fuselage.

5.1.5 Aileron effectiveness

The flight tests showed that the down going aileron was not effective at large deflections. To improve this the aileron hinge line was moved upwards (see fig. 12) to improve the flow on the aileron upper surface. The aileron effectiveness was improved and so was the linearity of the hinge moment curves, except at large deflections. The raising of the hinge line increased also the aileron up-float significantly and this was an additional reason for introducing the reflex upwards on the aileron fixed trailing edge.

A high pilot work load was initially experienced in turbulent approach conditions. In order to reduce the minimum control speed in landing the aileron effectiveness was improved through considerable flight testing by adding vortex generators on the aileron to re-energize the flow. The effect of the vortex generators was also tested in high speed

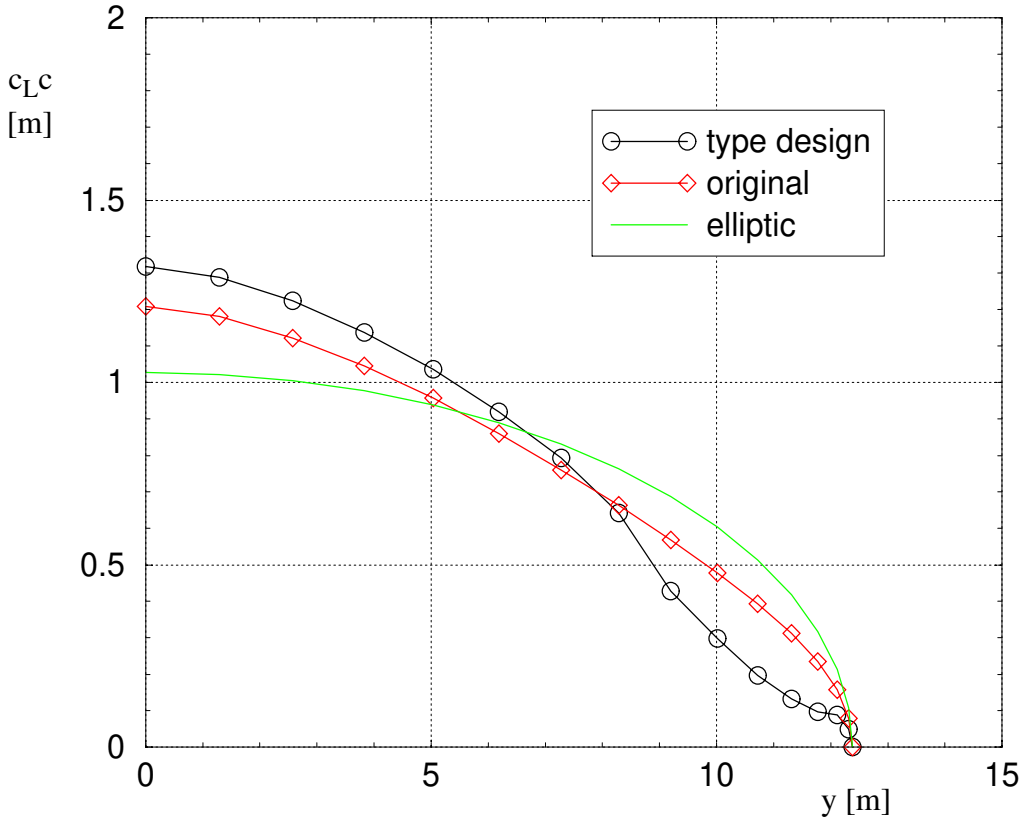

Figure 13. Lift distribution of Saab 2000 wing computed with extended lifting line theory. $\delta_a=0^o$, $\delta_f=0^o$, $C_L=0.359$, Ma=0.298. (ref. 54).

wind tunnel tests at FFA T1500 transonic tunnel. The maximum cross wind component in landing was increased from 26 kts to 40 kts, however only 3 years after the first flight. The final configuration of the vortex generators is shown in fig. 14.

A general problem for balanced ailerons is the reduction of hinge moments in sideslip, especially with flaps deflected, with a tendency for overbalance. After considerable experimentation the problem was solved with a nonlinear cam curve and by setting a fence on the upper surface at the aileron inboard edge. Putting the fence on the lower surface did not help. The sensitivity of the flow on the aileron behind the cut-out area is manifested by the fact that the upper aft fairing had to be left out.

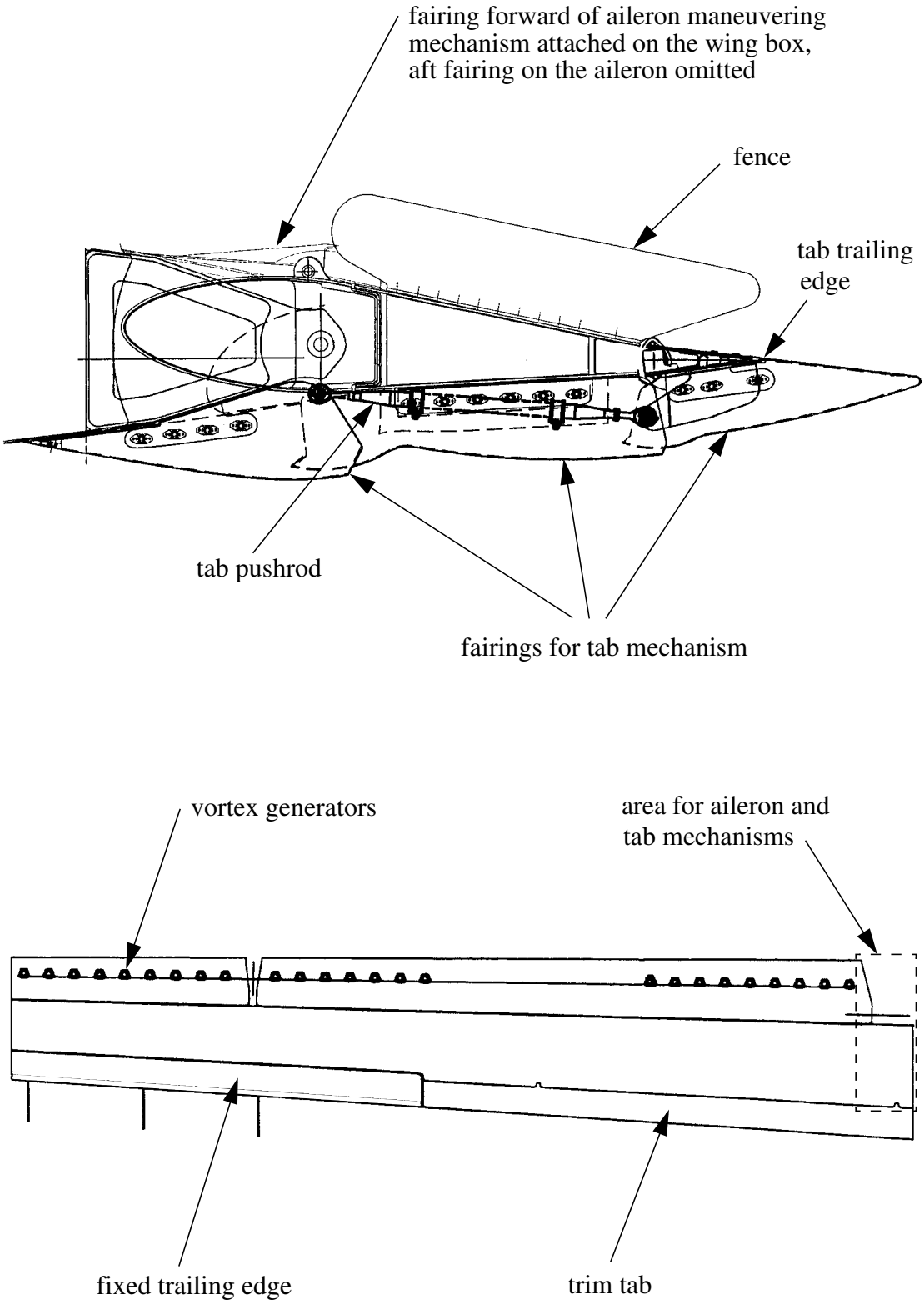

Figure 14. Overview on Saab 2000 type design aileron (ref. 54).

5.1.6 Control system mechanics

The tension in the control cables was reduced from 600 lbf to 300 lbf compared with Saab 340 to keep the wheel forces due to friction as low as possible. The airworthiness regulations do not set requirements on maximum breakout wheel force but Mil Spec (ref. 43) sets a value 6 lbf for category II land based light or medium transport aircraft. So of the maximum 25 lbf one hand wheel force 6 lbf may be due to friction and Saab 2000 fulfills this requirement. For control system description see paper V.

To ensure that full aileron deflections are reached during flight under loaded conditions the stops at the control wheel allow larger deflections on the ground than the stops at the ailerons. The difference is in the order of 5^o aileron deflection which means that the cables are relatively slack in normal operation. Consequently the gearing aileron/wheel deflection diminishes with increasing wheel force.

The close balancing of the ailerons means that the forces in the cables due to pilot forces are low. The load in the cables due to aerodynamic loads is however not low because the two ailerons work against each other and there may be a considerable hinge moment even at zero aileron deflection. The load induces wear in the cables.

The aileron hinge moments at flap deflection $\delta_f=15^o$ were almost the same as with flaps retracted but at 35^o flap the ailerons were considerably heavier. Eventually the problem was solved on 2000 with a variable tab gearing ratio depending on the flap deflection.

5.2 Analysis procedure

In the procedure of determining the aileron hinge moment two representative sections are taken through the aileron inner and outer parts. The local angles of attack in the sections are computed using the computer program LIFLI (ref. 37), based on the extended lifting line theory of Weissinger (refs. 67 and 68) developed further by DeYoung and Harper (ref. 14). The two-dimensional flow aerodynamic coefficients at the sections are computed using the Navier-Stokes code ns2d.

The creation of the computational grids were based on the experience gained in the investigations on grid variation and grid convergence. Plotting of the y^+ distribution showed that the value was fairly constant over the airfoil surface, see paper IV. The number of nodes was approximately 80000 on the aileron inner section and 74000 on the outer section giving run times of 3 to 7 days on Cray C90. An example of a grid is shown in paper VI. Convergence of the computations was checked by monitoring the rms values of the derivatives of the density and turbulent kinetic energy residuals as well as the aerodynamic coefficients of lift, drag and pitching and hinge moment. The derivatives of the residuals were not reliable indicators of convergence, as explained in paper VI. Due to small local time steps in the smallest cells the derivatives reached very high values. However, the absolute changes in the flow, not the derivatives, are of physical interest.

The transformation of the two-dimensional flow hinge moment coefficient to a three-dimensional value is based on the handbook method of ESDU. The method is based on determining the ratios of the derivatives in two- and three-dimensional flow of the linear-

ized hinge moment coefficient

$$c_h = c_{h_0} + c_{h_\alpha}\alpha + c_{h_\delta}\delta_a \qquad (26)$$

where c_{h_0} is the hinge moment coefficient at zero angle of attack and zero aileron deflection and the two other terms represent the effects of angle of attack α and aileron deflection δ_a. A correction due to the cut-outs at the aileron root and the hinge in the middle was performed.

The airplane rolling moment coefficient is also based on the handbook method of ESDU by feeding the CFD derived section lift effectiveness α_δ values into the calculations instead of using the empirical graphs for α_δ.

5.3 Comparison with flight tests

The validation cases were selected from the disconnect flight tests. The tests were performed by disconnecting the control system so that both ailerons could be deflected in the same direction. The airplane was kept in steady level flight at the specified flying speed and the aileron hinge moment was then measured on one (left) side. The chosen test flight with type design aileron configuration was performed at 180 KIAS with zero flap deflection. Because the flying speed was kept constant during the measurement the angle of attack decreased slightly when the ailerons were deflected downwards and vice versa.

The computed three-dimensional hinge moment coefficients for the aileron are presented together with flight test results in paper VI and fig. 15. The form of the computed curve matched better the flight test results for the aileron without vortex generators. This was as expected because no account was taken of the VGs in the two-dimensional modeling of the CFD computations. Because the wheel force is given by the difference of the left and right hand side hinge moments the slope, not the level of the curve is of primary interest.

The complete aileron is very closely balanced with the aerodynamic balance nose and the gearing of the tab. Actually the inner section is overbalanced due to the geared tab and works against the outer section. This means that the cut-outs at the root and in the middle, shown in figure 14, although being small in area, have a noticeable influence on the aileron hinge moment. Together they gave corrections of the same order of magnitude as the basic value. The aileron root part is difficult to model due to the fence on the upper side and the fairings on the lower side that modify the pressure distribution. The gaps in the cut-out area are so large that they permit a local flow of air through the structure. On the upper side the forward fairing causes a flow separation on the aileron over the entire width of the cut-out. It is difficult to take into account all these factors in the three-dimensional hinge moment coefficient. Considering the extremely low hinge moment values the case is really demanding and the results are surprisingly accurate even at -15^o and $+15^o$ aileron deflections.

The airplane rolling moment at 10^o aileron deflection, as calculated from the two-dimensional CFD computations and a transformation applying the method of ESDU, is 3% in excess of the flight test value with vortex generators and 29% in excess without vortex generators, see paper IV and table 1.

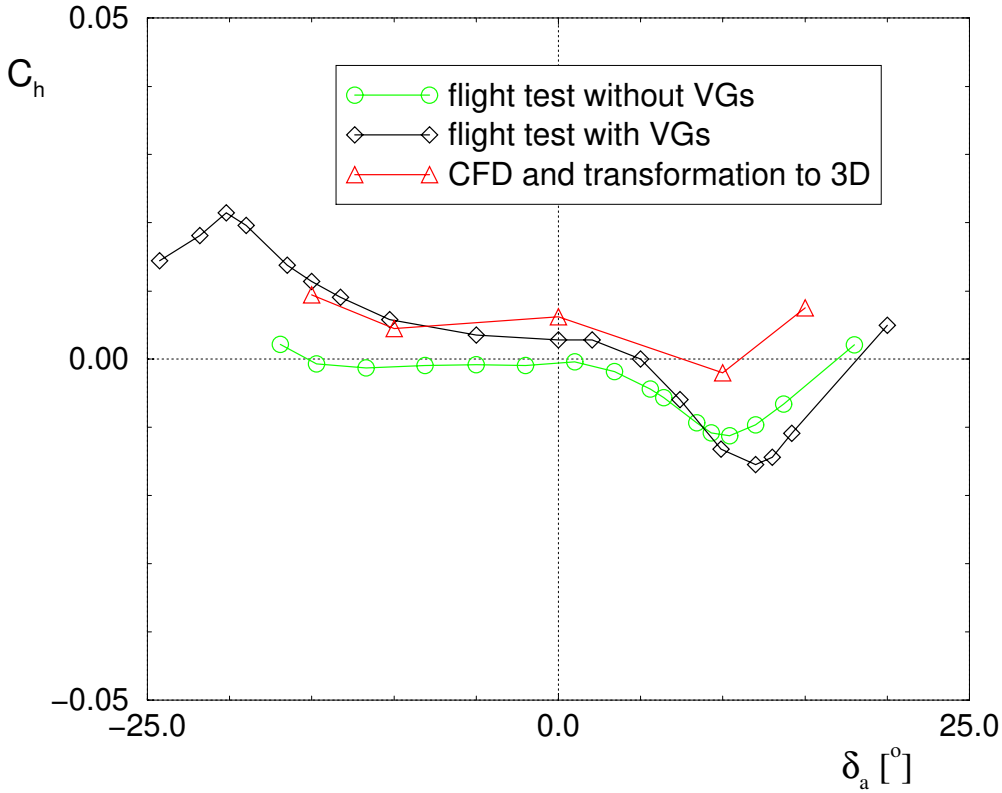

Figure 15. Comparison of hinge moment coefficients on Saab 2000 type design aileron without vortex generators, derived through CFD computations and flight tests. δ_f=0°, V=180 KIAS, trim tab deflection δ_{at}=-3° at zero aileron deflection. (ref. 57).

Table 1. Rolling moment coefficient at aileron deflections δ_{aL}=10° and δ_{aR}=-10° (ref. 54).

CFD and transformation	Flight Test	
ESDU, no VGs	no VGs	with VGs
0.0264	0.0205	0.0256

5.4 Effect of tolerances

The effect of the tab slot gap size was investigated by modeling the cavity in front of the tab, see fig. 16. The gap size was varied within the allowable production tolerances g=0.19 to 0.32% chord. The tab slot gap size had almost no effect on any of the sectional aerodynamic coefficients c_L, c_D, $c_{m.25}$ and c_h, see paper VI. As computations on nominal tab slot gap size with and without modeling the cavity showed very small differences at zero aileron deflection the effect of aileron slot gap size was studied without modeling the cavity.

On the aileron slot the constant width gap varies in the interval

minimum g=0.17...0.24% chord

maximum g=0.44...0.64% chord

with the low values referring to the aileron root and the high values to the tip. The nominal gap size varies between 0.34% and 0.49% chord. CFD computations were performed at the inner and outer aileron sections with different gap sizes. The effects on lift and hinge moment at the intentionally overbalanced inner section are depicted in fig. 17.

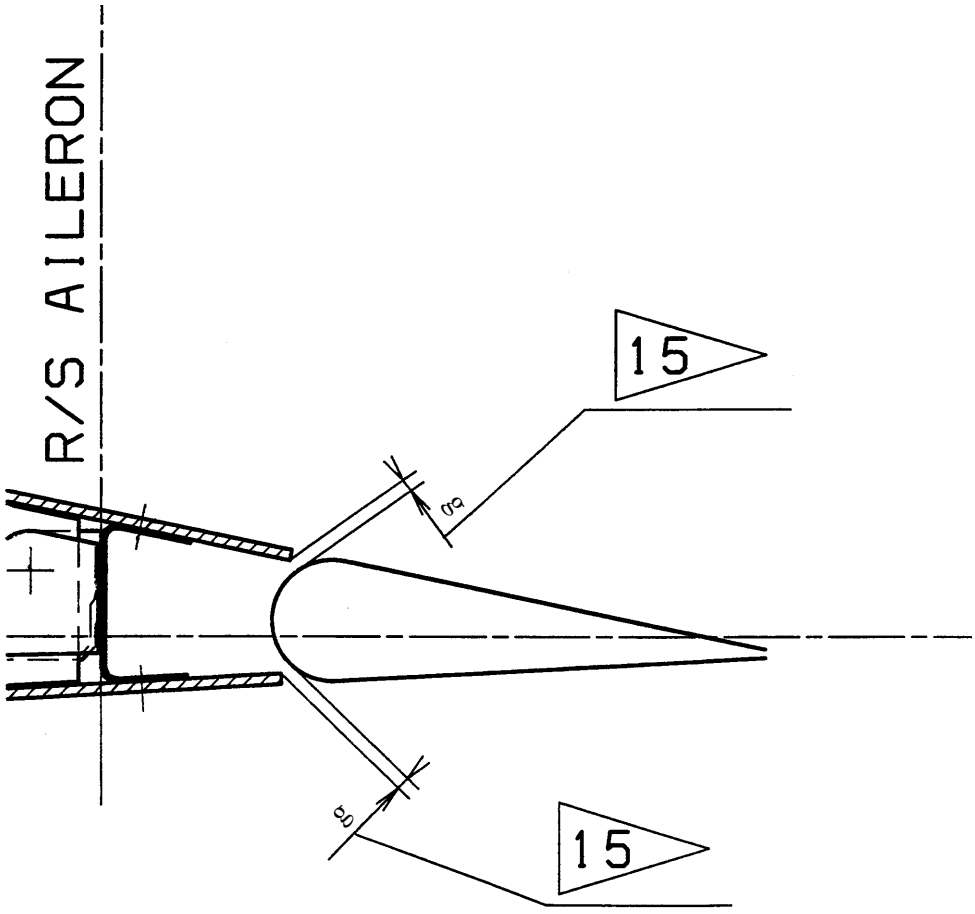

Figure 16. Saab 2000 aileron design at a section through the trim/geared tab, not to scale (ref. 57).

Increased gap size caused a noticeable loss of lift. The two-dimensional aileron effectiveness $\partial c_L / \partial \delta_a$ varied at positive aileron deflections in the tolerance band from -9% to +23% from the nominal value of 0.0319 per degree. At negative aileron deflections the variation was from -9% to +20%. The nominal value at negative deflections was 0.0327 per degree and consequently the unsymmetry at positive and negative aileron deflections gave a ratio of 0.98 on aileron effectiveness. It is to be noted that the computed values contain the effect of tab gearing. The fixed trailing edge on the outer section gave considerably higher effectiveness. Contrary to the rule of thumb of Morgan&Thomas (ref. 46) the slot does not seem to be "effectively sealed from the viewpoint of lift" below g=0.25% and "effectively fully unsealed" beyond 0.5% chord.

The influence of aileron slot gap size on the sectional hinge moment coefficient varied at $+10^o$ deflection from 0.0091 to -0.0024 corresponding to the minimum and maximum gap widths respectively. At -10^o deflection the corresponding values were -0.0042 and 0.0027. The increase of the aileron slot gap size steepens the net hinge moment curve and thus increases the wheel forces. This is also true about the outer aileron section where the hinge moment values were higher due to the fixed trailing edge.

The flow patterns at -10^o and 0^o aileron deflections were principally the same for the minimum and maximum gap sizes. However, the flow through the aileron slot changed direction between the deflections -10^o and 0^o. With the maximum gap size the increased flow through the slot required more volume and hence diminished the vortices in the aileron slot area. At 10^o aileron deflection the flow patterns differed on the aileron upper surface (fig. 18). On the minimum gap geometry there was a small vortex on top of the aileron balance nose but no flow separation in front of the tab slot. The maximum gap geometry showed no flow separation on the balance nose (even if the flow was locally retarded with a thickened boundary layer). In front of the tab slot there was a local region of separated flow. Computations with the nominal gap size showed a vortex on the balance nose and a barely visible beginning flow separation in front of the tab slot (fig. 19). The vortex in front of the tab slot was not present at aileron deflections -10^o and 0^o. Together with the change of the flow direction through the aileron slot the unsteady vortex might cause oscillations of the aileron.

With the original low hinge axis position and the nominal gap size there was a flow separation on the aileron upper surface in front of the tab slot. Due to the raised hinge line the flow separation was successfully delayed with an improvement in aileron effectiveness. The two-dimensional aileron effectiveness $\partial c_L / \partial \delta_a$ was increased by 12% at positive deflections and reduced by 2% at negative deflections. The ratio of sectional aileron effectiveness at positive and negative deflections was improved from 0.858 to 0.978. According to the computations the raise of the hinge line gave a drag reduction amounting to 7 drag counts with the ailerons in the neutral position.

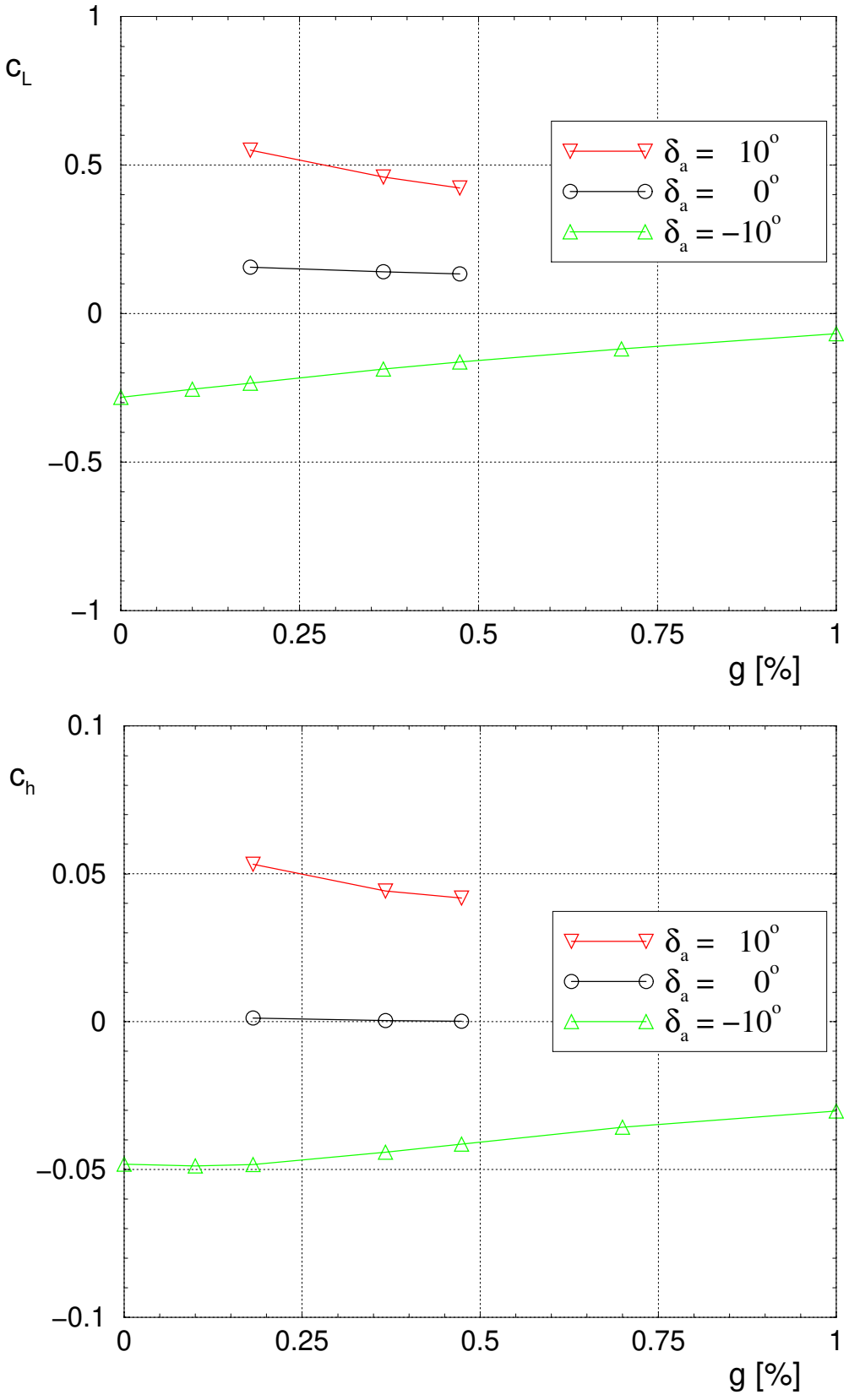

Figure 17. Effect of aileron slot gap size g on two-dimensional flow lift and hinge moment coefficients on the inner section of Saab 2000 type design aileron. $\alpha=0^{o}$, Ma=0.298, $Re=10.7\cdot10^{6}$ (ref. 57).

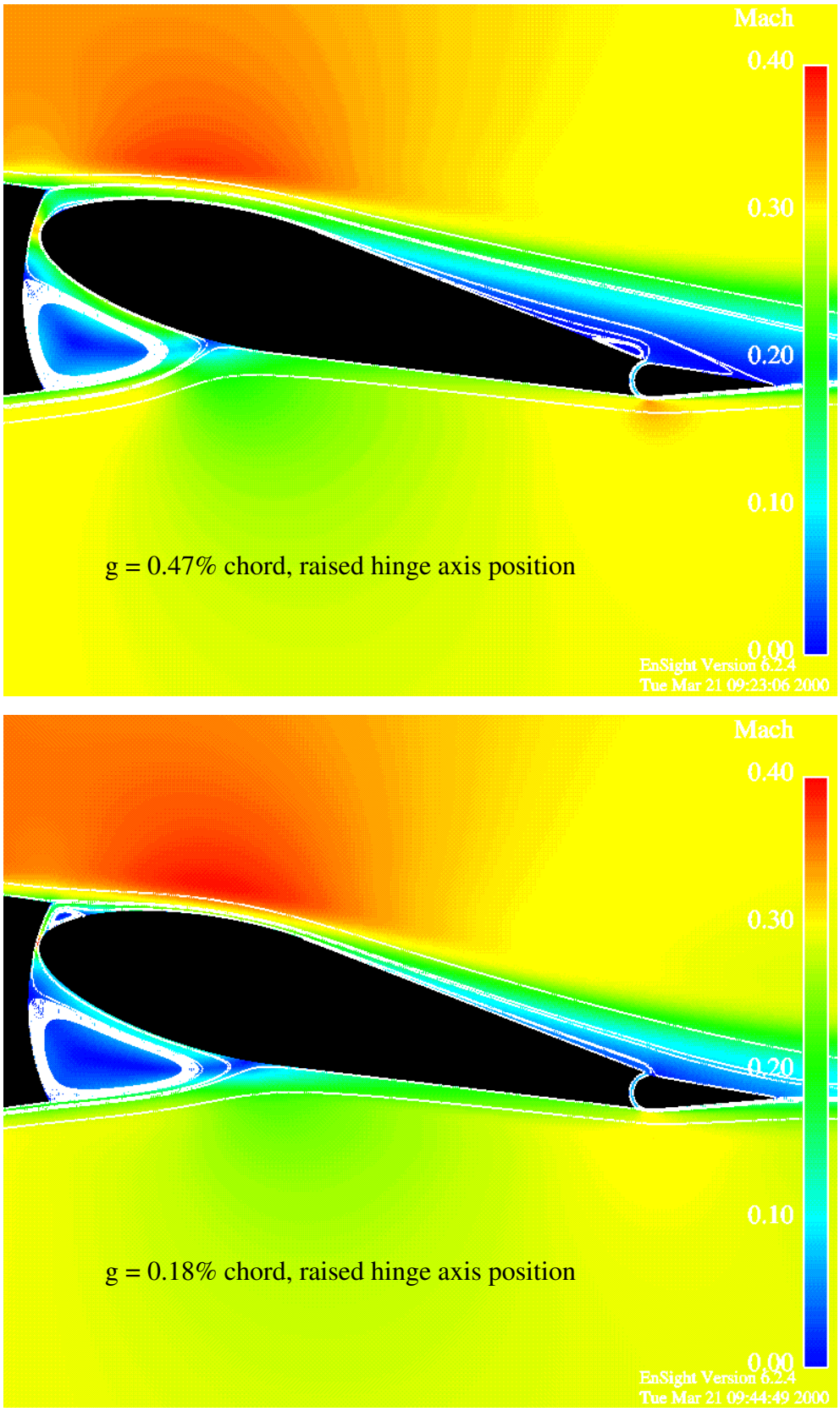

Figure 18. Mach number distribution and streamlines around aileron inner section with minimum and maximum gap sizes at aileron deflection 10^{o}. $\alpha=0^{o}$, Ma=0.298, $Re=10.7\cdot10^{6}$. Two-layer turbulence model (ref. 57).

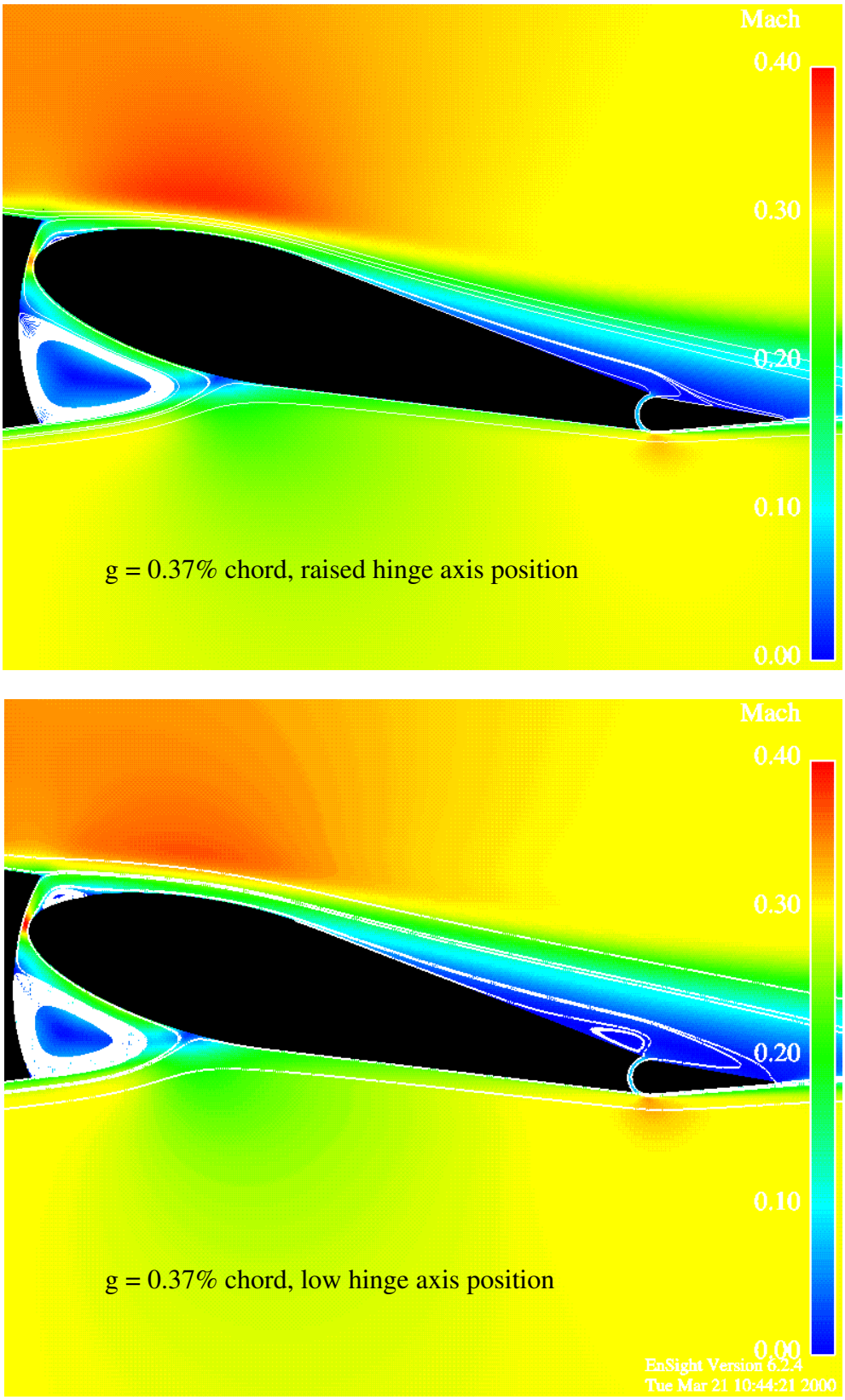

Figure 19. Mach number distribution and streamlines around aileron inner section with nominal gap size at aileron deflection 10^{o}. $\alpha=0^{o}$, Ma=0.298, Re=$10.7 \cdot 10^{6}$. Two-layer turbulence model (refs. 54, 57).

6. FLIGHT DYNAMIC DESIGN OF AILERONS

6.1 Flight mechanical simulations

6.1.1 Simulation system

FORMIC is the simulation system used at Saab for flight mechanical simulations on Saab 340 and Saab 2000 aircraft (ref. 5). The aircraft models, linked together with FORMIC, are based on state space representation of the flight mechanical six degree of freedom differential equations, the airplane control system, landing gear, engines and other pertinent systems. Nonlinearities in the aerodynamic data are fully taken into account. The flight mechanical modeling has been verified through comparison with flight test maneuvers in proof of match tests, required by the authorities for the airplane simulator for pilot training.

In the state-space representation the higher order flight mechanical differential equations and other differential equations included into the system are transformed into a set of first order differential equations that are written in matrix form

$$\dot{x} = Ax + Bu \tag{27}$$

where x is the state vector, $\dot{x}$ its derivative and u is the vector of control inputs. A is the plant matrix and B the control or input matrix. The output of the system is expressed in terms of the state and control inputs as follows:

$$y = Cx + Du \tag{28}$$

where y is the output vector and C and D the appropriate system matrices. Equations (27) and (28) are solved by numerical integration. A version of the Runge Kutta 3rd order integration method, modified by Ashour for better performance on stiff equations (ref. 3), is used. The program automatically adjusts the integration step so that the specified accuracy is reached.

The basic flight mechanical equations in the airplane models are written by treating the earth as a stationary plane in inertial space. The force balance is written in body axes (the index b is left out)

$$X - mg\sin\theta = m(\dot{u} + qw - rv) \tag{29}$$

$$Y + mg\cos\theta\sin\phi = m(\dot{v} + ru - pw) \tag{30}$$

$$+ mg\cos\theta\cos\phi = m(\dot{w} + pv - qu) \tag{31}$$

where X, Y and Z are the aerodynamic forces acting in the direction of body axes x, y and z respectively, shown in fig. 20. m is airplane mass and g the gravity of earth. θ is the elevation angle and ϕ the bank angle. u, v and w are the components of the airplane speed projected to the x, y and z axes respectively with dots indicating the corresponding accelerations. p, q and r are angular rates around the x, y and z axes respectively.

The moment balance is written in the body axes

$$L = I_x\dot{p} - I_{zx}(\dot{r} + pq) - (I_y - I_z)qr \tag{32}$$

$$M = I_y\dot{q} - I_{zx}(r^2 - p^2) - (I_z - I_x)rp \tag{33}$$

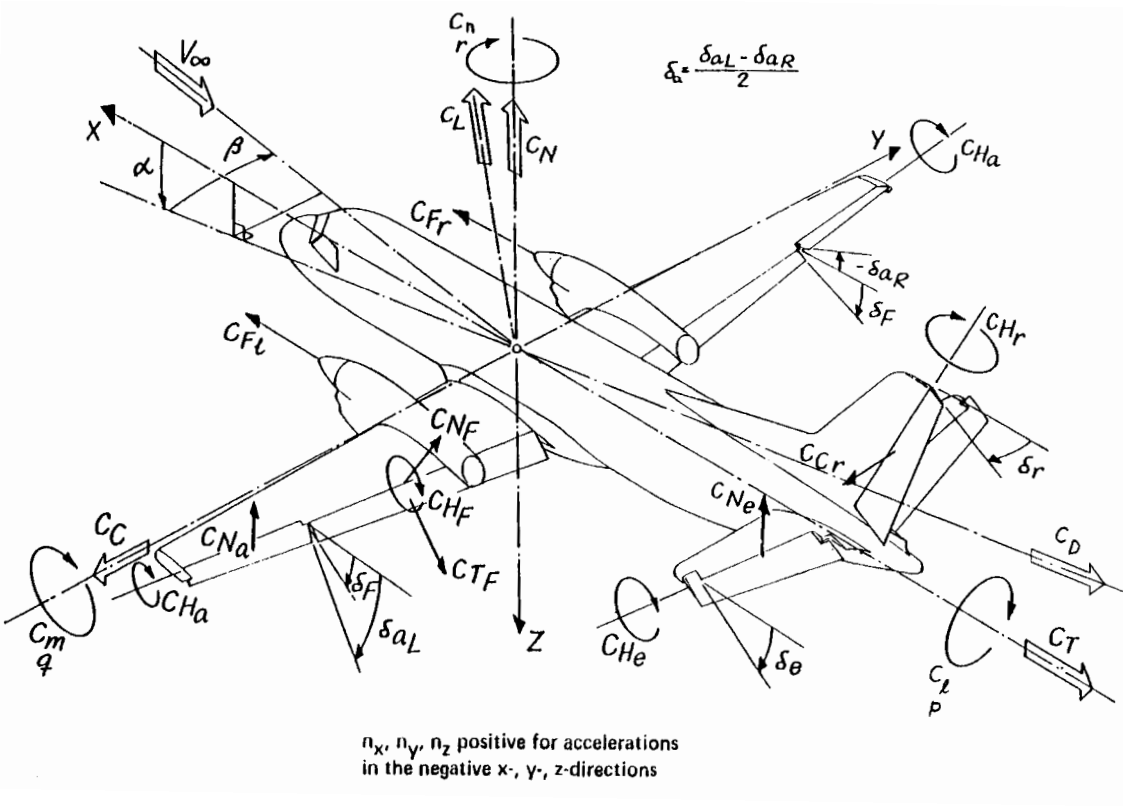

Figure 20. Positive directions for flight mechanical entities in the Saab system. Notice that the system is not identical with that of Etkin (refs. 23, 59). In the Saab system for example the side force coefficient C_C is defined in body axes and both aileron deflections are defined positive trailing edge down.

$$N = I_z\dot{r} - I_{zx}(\dot{p} - qr) - (I_x - I_y)pq \tag{34}$$

where L, M and N are the aerodynamic moments acting around the body axes x, y and z respectively. The moments of inertia are denoted with I with an obvious convention for the indices. A dot on the angular rates indicates time derivative yielding corresponding angular accelerations.

The Euler angle rates are obtained from kinematics in body axes

$$\begin{bmatrix} \dot{\phi} \\ \dot{\theta} \\ \dot{\psi} \end{bmatrix} = \begin{bmatrix} 1 & \sin\phi\tan\theta & \cos\phi\tan\theta \\ 0 & \cos\phi & -\sin\phi \\ 0 & \sin\phi\sec\theta & \cos\phi\sec\theta \end{bmatrix} \begin{bmatrix} p \\ q \\ r \end{bmatrix} \tag{35}$$

where ϕ is bank angle, θ elevation angle and ψ azimuth angle.

Also from kinematics are obtained relations for the angle of attack α and the sideslip angle β

$$\alpha = \operatorname{atan}\frac{w_a}{u_a} \tag{36}$$

$$\beta = \operatorname{atan}\frac{v_a}{\sqrt{u_a^2 + w_a^2}} \tag{37}$$

where u_a, v_a and w_a are the airplane atmospheric (true) airspeed components projected into the body oriented system. The positive directions of α and β are shown in fig. 20.

The aircraft position in earth coordinates x_E, y_E and z_E is obtained by applying a general coordinate transformation from the speed vector $[u\ v\ w]^T$ in body axes to the speed vector $[\dot{x}_E\ \dot{y}_E\ \dot{z}_E]^T$. The earth coordinates, denoted with the index E, are body fixed but parallel with the earth defined axes in order to simplify coordinate transformations with respect of acceleration terms. A fourth coordinate system t, based on the airplane trajectory, is used in the calculations because it simplifies the trimming (longitudinal and lateral equations).

The differential equations (29) to (34) contain all forces and moments inclusive those of the airplane controls, such as ailerons, and are integrated in time using the relations of other pertinent equations. The basic entities in the state vector are the airplane position coordinates x_E, y_E and z_E, speeds u, v and w, Euler angles θ, ϕ and ψ and the rotation rates p, q and r. Because the flight mechanical equations can be split into the longitudinal and lateral equations the state vectors are also handled separately. This simplifies trimming the model and permits three degree of freedom simulations. The longitudinal motion basic state vector contains entities u, w, q and θ and the lateral motion basic state vector v, p, r, and ϕ.

6.1.2 Aileron control system modeling

The differential equation for the motion of two ailerons without aileron differential and lying in xy-plane can be expressed (see ref. 24)

$$I_a\ddot{\delta}_a + 2P_{ay}(rq + \dot{p}) = 2H_a + F_a \tag{38}$$

where I_a is the aileron moment of inertia around the hinge axis, δ_a aileron deflection, P_{ay} the product of inertia of the aileron with respect to its hinge line and the x axis, H_a hinge moment of one aileron and F_a generalized aileron control force.

For the purpose of modeling the aileron control system it was divided into seven mass points which were connected together with weightless springs, see fig. 21. Because account was taken of the aileron differential, asymmetric aerodynamics on the left and right hand sides etc one equation was needed for every mass point. This meant that an equation similar to the above equation was written for every mass point so that there was a set of seven differential equations. Due to the nonlinearities and backlashes in the control system it was possible to solve the system of equations only numerically.

Friction exists at the control wheels, along the control path at the pulleys and at the ailerons. The friction function uses a basic static friction level, denoted with H_F for the

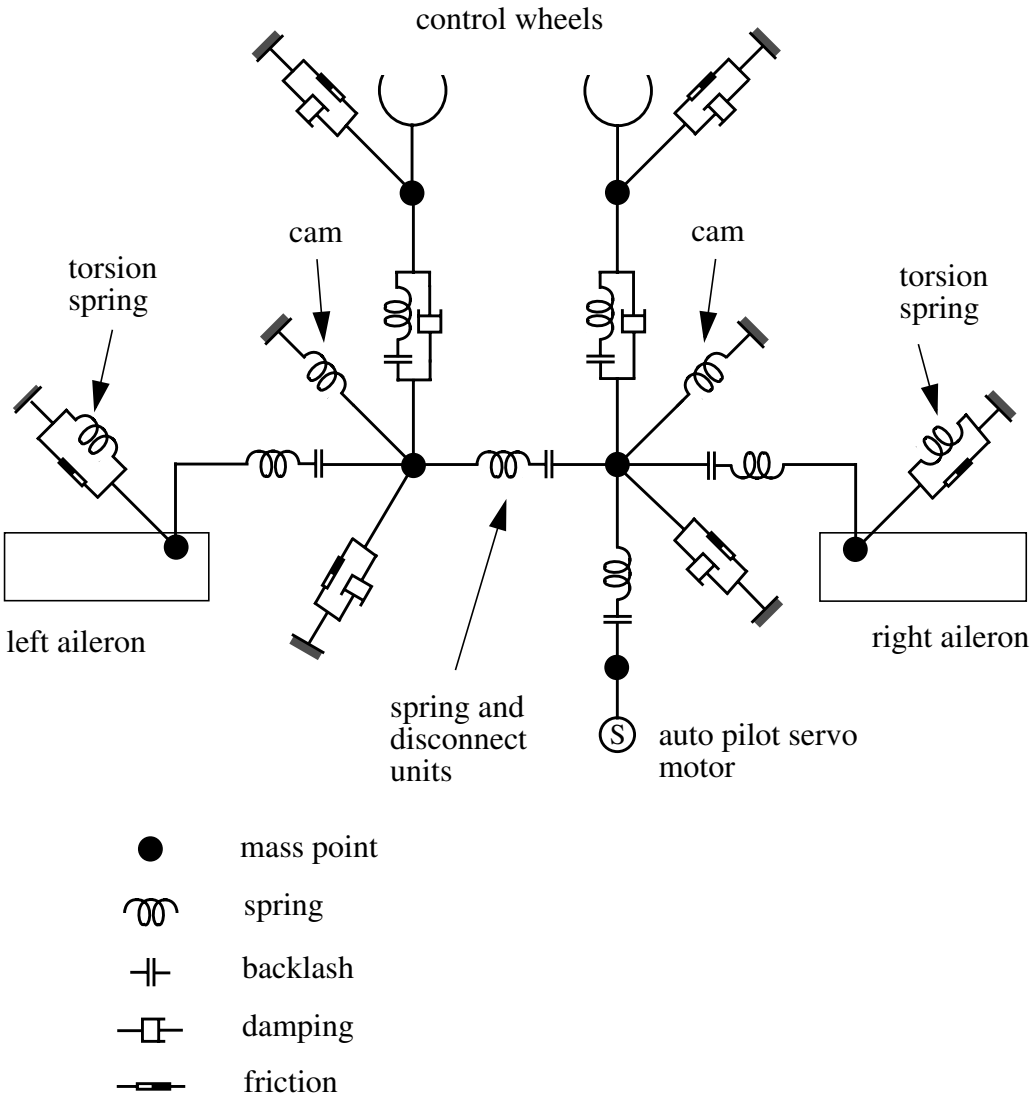

Figure 21. Aileron control system model on Saab 2000 (ref. 59).

corresponding (local) moment, and the (local) deflection rate $\dot{\delta}$ as inputs. It provides static friction, starting friction and dynamic friction depending on the deflection rate in question. The friction curve is presented in paper V.

Besides the aerodynamic damping of the ailerons also the small damping in the control path itself due to corrosion protection grease on the cables and the chain in the control column was taken into account. The damping functions were linear with respect of the local deflection rate $\dot{\delta}$. Backlashes in the control system were taken into account by modeling them as very weak and aileron stops as very stiff springs.

The nonlinear behavior of the centering cams, disconnect and spring units, aileron differential as well as nonlinear aerodynamic data were accurately taken into account in the modeling. The geared tab and spring tab were not modeled with a mass point but the tab

deflection was calculated arithmetically as well as the loads from the tabs (and associated springs) to the aileron. The modeling of the control system has been verified by ground response tests.

The aerodynamic data for Saab 2000 and 340 type design configurations were taken from the pertinent Aerodynamic Design Data Books (ADDB), based on wind tunnel experiments and verified through flight tests. Simulations on Saab 2000 were also made on an aileron configuration without Vortex Generators. The aerodynamic data without VGs was based on two-dimensional Navier-Stokes computations. The two-dimensional flow aerodynamic coefficients on aileron hinge moment and airplane rolling moment were transformed into 3D values using the handbook method of ESDU.

Aerodynamic data for the simulations on the effects of aileron slot gap size was based on the type design values. Corrections were made on aileron hinge moment coefficients, where the changes due to the aileron slot size on the inner and outer sections were weighed together. Also the airplane rolling moment values due to aileron deflection were adjusted accordingly.

6.1.3 Steady heading sideslips

Lateral static stability was investigated in steady heading sideslip. Paragraph 25.177 of FAR 25 (ref. 26) requires that the static lateral stability, as shown by the tendency to raise the low wing in a sideslip with aileron controls free may not be negative. Further the aileron control movements and forces in straight, steady sideslips must be substantially proportional to the angle of sideslip (within sideslip angles appropriate to the operation of the airplane). The case with flaps at $\delta_f=35^o$ was investigated landing gear down and with power for level flight (PFLF). The airplane weight was chosen as 19000 kg (42000 lbs), center of gravity position at 37% MAC and flying speed 165 KCAS, a flight test case at maximum flaps extended speed V_{FE}.

An extract of the simulation results in fig. 22 shows that up to sideslip angles of 5^o the computations, based on the hinge moment derived through CFD and a transformation to 3D, are close to the results of the type design aileron with vortex generators. At large sideslip angles the computed wheel force changes sign indicating that the control wheel would go against a stop when released free. The phenomenon was noticed in development flight tests on an aileron configuration without the fence and vortex generators.

Simulations were also carried out for a spring tab configuration with and without the effect of vortex generators. The wheel force curve is more nonlinear than for the type design configuration because the cam curve, tailored for the type design ailerons, was not changed. However, the difference in the wheel force for the spring tab configuration with and without VGs is considerably smaller than in the case of the type design aileron with the geared tab. This shows that the self adjusting spring tab is capable to compensate for changes in the aerodynamic hinge moment.

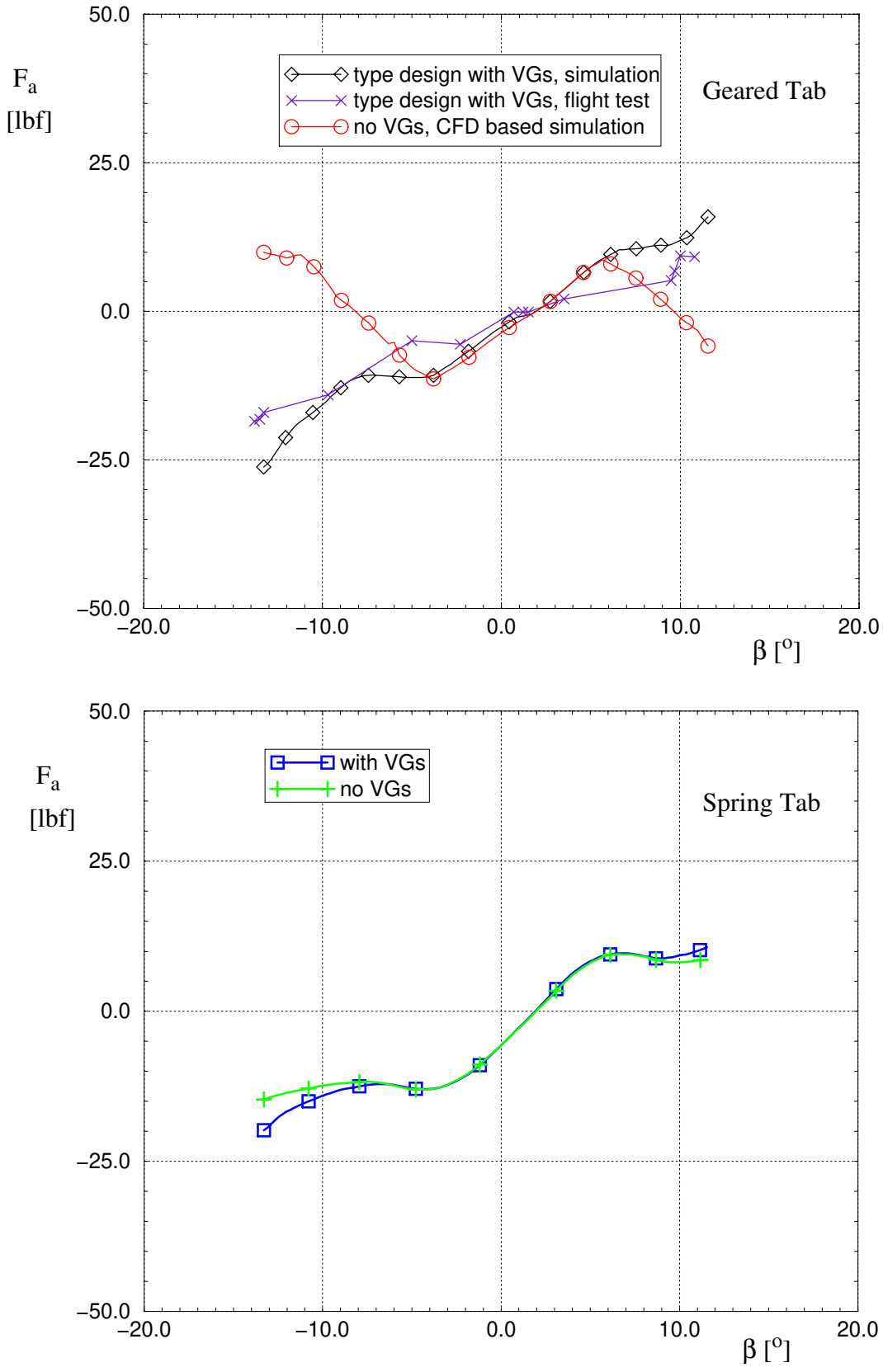

Figure 22. Wheel force F_a on Saab 2000 with geared tab and spring tab ailerons as function of sideslip angle at V_{FE}=165 KCAS, δ_f=35°, landing gear down and PFLF (ref. 59).

6.1.4 Roll maneuvers

Roll control efficiency was investigated at low speed in an approach condition and at high speed in an enroute condition where ACJ 25.147(e) of JAR 25 (ref. 32) requires a roll of 60^o from a steady 30^o banked turn so as to reverse the direction of turn in not more than 7 seconds.

At low speed a flight test case was investigated at a weight of 21550 kg (47500 lbs) corresponding to a reference speed of V_{REF}=119 KCAS (1.3 V_{S1}). The airplane was trimmed to give a 5% gradient of descent. An extract of the simulation results in fig. 23, with the control wheel deflections from 10^o to 70^o, showed that the omission of VGs gave a reduction of wheel forces with a tendency for overbalancing. The abrupt increase of the wheel force in the fastest roll maneuvers was due to aileron bottoming. The same simulations were also performed on the spring tab configuration. With the vortex generators the spring tab system gave a faster roll at a specified wheel force.

At high speed a flight test case was investigated at the maximum operating speed V_{MO}=270 KCAS at 15000 ft. The airplane weight was 21280 kg (46900 lbs) with the CG position at 37% of MAC. The flaps and landing gear were retracted and the power setting was set at power for level flight (PFLF). The simulations for the geared tab configuration in fig. 24 showed a fairly good matching on the wheel force between the simulations and flight tests with vortex generators. On the spring tab configuration the wheel forces were low even at the highest applied wheel deflection of 70^o. The spring tab configuration was clearly less sensitive to the aerodynamic hinge moment changes due to the vortex generators and could in the high speed flight case compensate for the effects of flying speed.

The investigated dimensioning cases on one hand of the steady sideslips and low speed roll maneuvers and on the other hand the high speed roll maneuvers, based on the investigation of ref. 56, represent the extreme cases for wheel force. At low speed the wheel forces were low or even reversed sign and at high speeds the forces were high.

The effect of aileron slot gap size variation on roll maneuvers was investigated at V_{MO} in the same flight condition that was used to study the effects of aileron rigging tolerances (ref. 57). The flight altitude was chosen from the altitude-speed envelope as the lowest altitude, 11000 ft, where the maximum operating speed 270 KEAS is allowed. The total wheel force and the wheel force due to the aerodynamic hinge moment for the geared tab configuration are shown in fig. 25 as function of the time needed to roll the required 60^o. Wheel force values due to all allowed production tolerances, measured in production aircraft, are shown as comparison. According to the simulations in ref. 57 the variation in wheel force due to aileron slot gap size somewhat exceeds the variation due to the allowed tab rigging tolerances. The variation in wheel force was considerably smaller on a spring tab configuration, see paper VI.

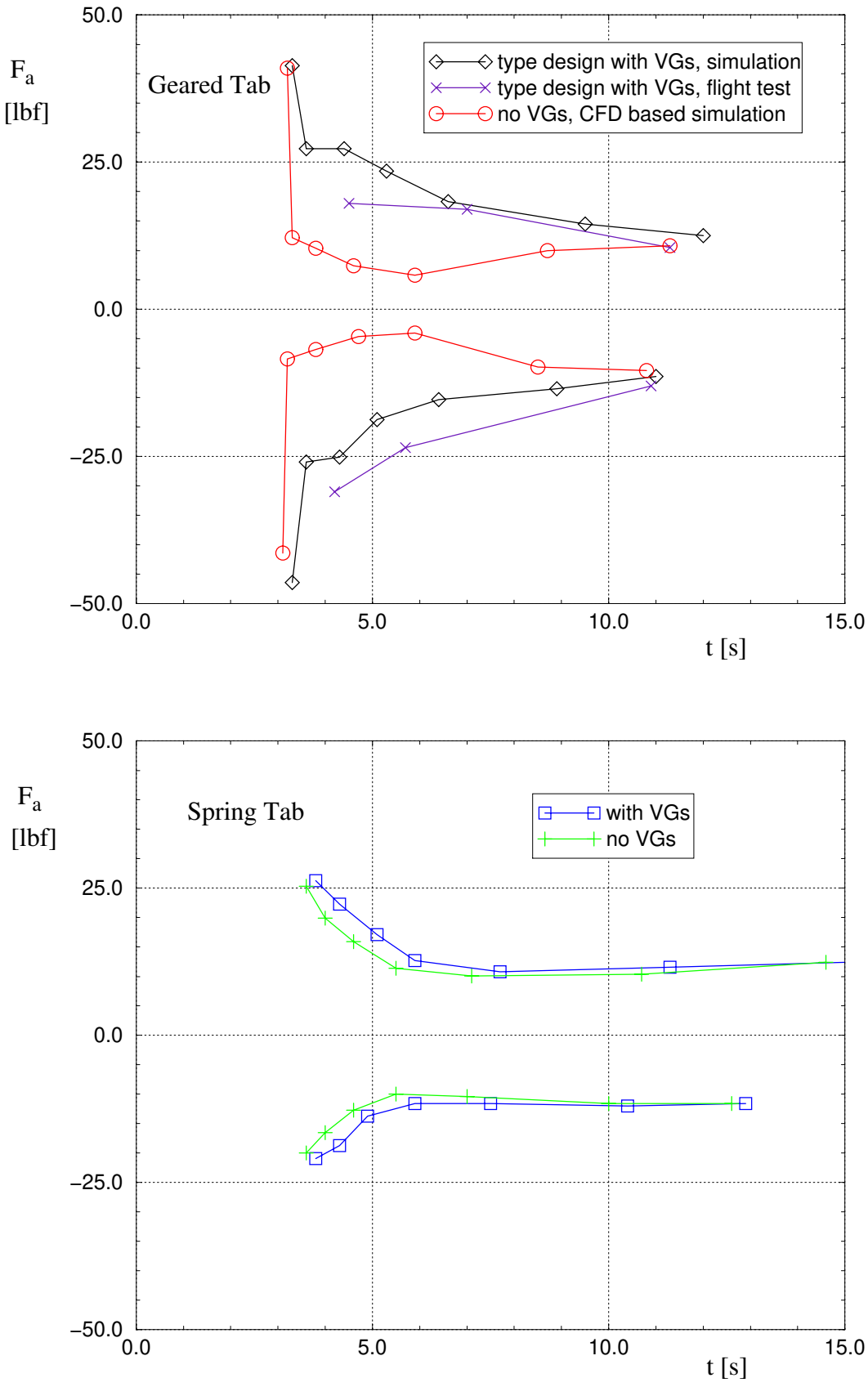

Figure 23. Wheel force on Saab 2000 with geared tab and spring tab ailerons as function of time in a 60° roll maneuver at 119 KCAS, δ_f=35°, landing gear down, power for 5% descent (ref. 59).

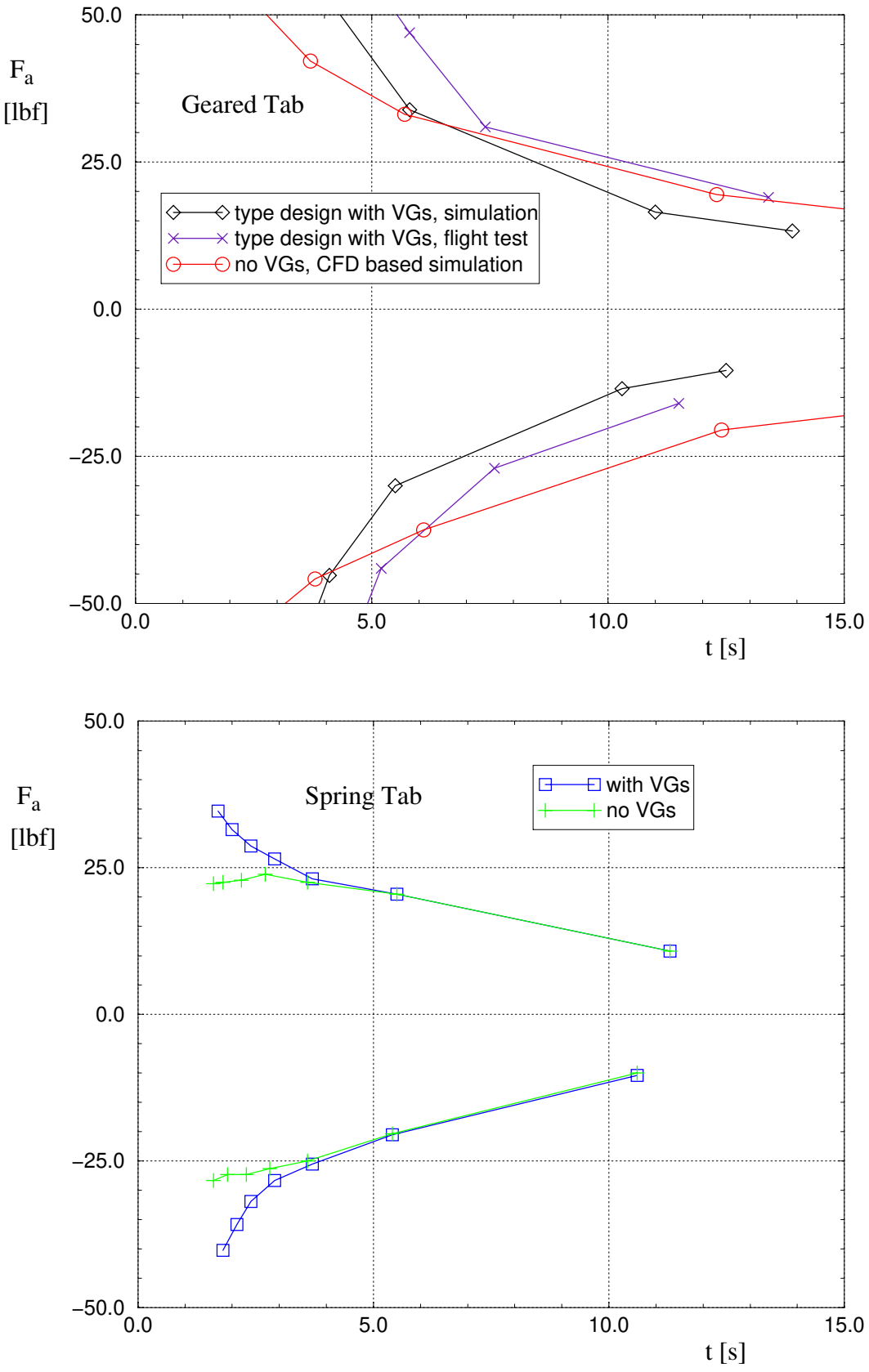

Figure 24. Wheel force on Saab 2000 with geared tab and spring tab ailerons as function of time in a 60° roll maneuver at 270 KCAS, flaps and gear retracted, PFLF (ref. 59).

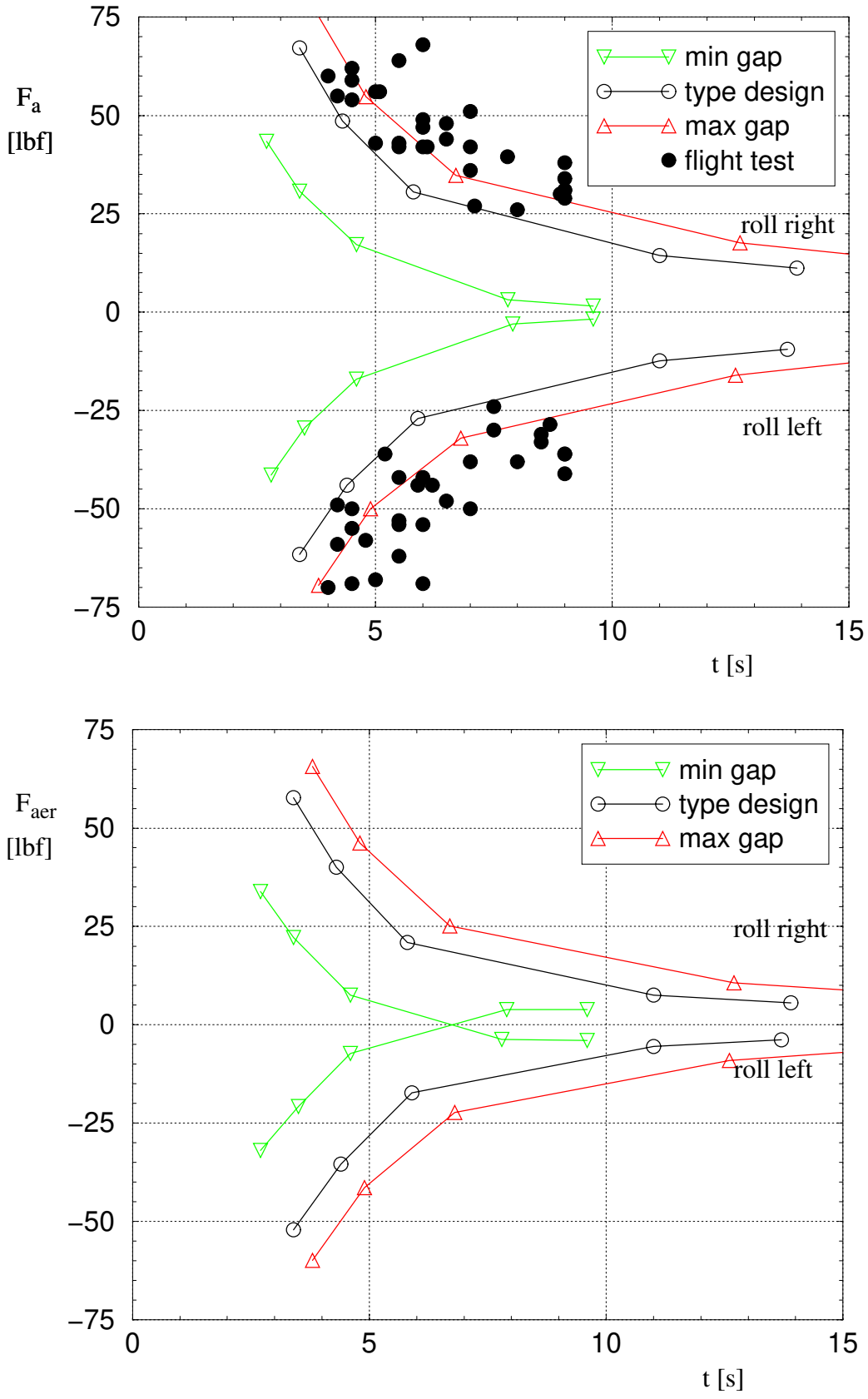

igure 25. Effect of aileron slot gap size on wheel force F_a and aerodynamic wheel force F_{aer} on Saab 2000 with a geared tab aileron as function of time to roll 60° at V_{MO}=27 KCAS, δ_f=0°, landing gear up, PFLF (ref. 57).

6.2 Frequency analysis

6.2.1 Outline of procedure

Frequency analysis was used to study the response of aileron deflection, airplane roll rate and roll acceleration to the wheel force applied by the pilot. The applied wheel force was modeled using a chirp signal with varying frequency. The response of the system in time was determined with the simulation system FORMIC that produces the output signal at selected discrete time steps. The frequency response was calculated using Fourier analysis, spectrum analysis and system identification employing an ARX model.

Simulink system was used to create a 10 second long signal with an initial frequency of 0.1 Hz and a final frequency of 2.0 Hz. The frequency interval was chosen to cover the interesting area of human pilot operation in gusty weather that is known to be around 1 Hz. The amplitude of the wheel force was chosen as 22.5 lbf (100 N). This is just below the value 25 lbf that is the maximum limit set by the airworthiness authorities in approach flight with only one hand operation. By increasing the sampling frequency until the frequency response results did not change anymore a frequency of 80 Hz was chosen.

The flight case chosen for the studies is approach flight on a 3^o glide slope at an altitude of 1000 ft flaps deflected 35^o at the lowest value of minimum control speed in landing V_{MCL}. The speeds and corresponding airplane weights are

	V_{MCL}	W
	[KIAS]	[lbs]
Saab 340	106	20000
Saab 2000	111	40800

Besides the effect of aileron and tab deflections on the aileron hinge moment coefficient, account was taken on angle of attack and sideslip, flap angle, power and dynamic effects. The majority of the aerodynamic data is verified through flight tests and a smaller extent is based on wind tunnel tests.

The deflection rate derivative is quite important as it is known to often supply the main damping of the aileron control system. The value of the derivative on Saab 2000 was identified from flight tests. As there was no flight test value on 340 a new estimate was computed using Saab´s unsteady potential flow code Aerel that was calibrated with the 2000 flight test data. For more details on the dynamic derivatives see paper V.

6.2.2 Fourier analysis

The transfer function G(q) of a general linear model

$$y(t) = G(q)u(t) + v(t) \tag{39}$$

can be estimated with Fast Fourier Transform (FFT) when the input and output vectors, u(t) and y(t) respectively, are known in discrete form vectors. q is the shift operator

$$qy(t_k) = y(t_{k+1}) \tag{40}$$

and v(t) is a noise term.

The empirical transfer function estimate can be calculated as

$$\hat{G}_S(i\omega) = \frac{Y_S(\omega)}{U_S(\omega)} \tag{41}$$

where

$$Y_S(\omega) = \sum_{k=1}^{N} y(t)e^{-i\omega kT} \tag{42}$$

$$U_S(\omega) = \sum_{k=1}^{N} u(t)e^{-i\omega kT} \tag{43}$$

with sampling data available at time periods kT, with k=1...N. The estimates $Y_S(\omega)$ and $U_S(\omega)$ were be computed using Discrete Fourier Transform formulas that employ the recursive formulas of Fast Fourier Transform (ref. 50).

Comparing the state space representation of the flight mechanical differential equations and the equations for the aileron control system, equations (27) and (28) on page 49, it is seen that in transfer function form the equations for the state space representation correspond with

$$G(q) = C(qI - A)^{-1}B + D \tag{44}$$

where I is identity matrix.

6.2.3 Spectrum analysis

Provided that the input u(t) is independent of noise v(t) the linear system equation (39) implies for the associated spectra

$$\Phi_{yu}(\omega) = G(e^{i\omega})\Phi_u(\omega) \tag{45}$$

Consequently the frequency function $G(e^{i\omega})$ can be estimated by estimating the two spectra. This was done using

$$\hat{\Phi}_{yu}(\omega) = \sum_{\tau=-M}^{M} \hat{R}_{yu}(\tau)W_M(\tau)e^{-i\omega\tau} \tag{46}$$

where the covariance function was estimated

$$\hat{R}_{yu}(\tau) = \frac{1}{N}\sum_{t=1}^{N} y(t+\tau)u(t) \tag{47}$$

The formulas for the other spectrum are analogous. $W_M(\tau)$ is the so-called lag window

$$W_M(\tau) = \int_{-\pi}^{\pi} w(\xi) e^{i\xi\tau} d\xi \tag{48}$$

and M is the width of the window. Here a Hamming window

$$w(\xi) = \frac{1}{2}\left(1 + \cos\frac{\pi\xi}{M}\right) \qquad |\xi| < M \tag{49}$$

$$w(\xi) = 0 \qquad |\xi| \geq M \tag{50}$$

with a window size equal to the entire data length was used.

When a time continuous system is approximated with a discretely sampled system there is a difference between the time continuous frequency function $G(i\omega)$ and the sampled frequency function $G_T(e^{i\omega t})$. Even if the frequency functions give exactly the same output at a sample time period t_k, the functions are not exactly the same. As a rule of thumb it can be said that the agreement is good up to a frequency of a tenth of the sampling frequency (ref. 36).

6.2.4 System identification

Parametric model estimation utilizes rational functions for the modeling of the transfer function. The ARX model is usually written

$$A(q)y(t) = B(q)u(t - nk) + e(t) \tag{51}$$

where A and B are polynomials in the delay operator q^{-1}

$$A(q) = 1 + a_1 q^{-1} + \ldots + a_{na} q^{-na} \tag{52}$$

$$B(q) = b_1 + b_2 q^{-1} + \ldots + b_{nb} q^{-nb+1} \tag{53}$$

The transfer function then reads

$$G(q) = q^{-nk}\frac{B(q)}{A(q)} \tag{54}$$

The model structure is set by the three constants na, nb and nk that define the order of the polynomials in the numerator and denominator respectively and the number of time delays. The time delay in the discrete model corresponds to the difference in the orders of the differential equations representing the wheel force pulse (the denominator) and the airplane dynamics (the numerator) in the continuous model.

A low order model was preferred because higher order models tend to develop local maxima in gain at high frequencies. This was especially true for high values of nb as the order of modeling for the aileron deflection was increased. It was more important to have a higher value for na that describes the airplane dynamics. The order of time delays was chosen to minimize the loss function.

Because the model was validated on the same data set from which it was estimated

Akaike´s Final Prediction Error (FPE) was chosen to minimize the variance of the prediction error. The FPE is expressed as

$$\frac{1 + n/N}{1 - n/N} \frac{1}{N} \sum_{t=1}^{N} \varepsilon^2 \tag{55}$$

where n is the total number of estimated parameters, N is the length of the data record and ε is the prediction error

$$\varepsilon(t, \theta) = y(t) - \hat{y}(t, \theta) \tag{56}$$

with $\hat{y}(t, \theta)$ being the estimate of y(t) depending on the model θ.

Also the standard deviations of the polynomial coefficients of A(q) and B(q) were monitored. It showed that when the high order models developed local maxima of gain at high frequencies the standard deviations were high, sometimes even higher than the polynomial coefficients themselves. This was an indication on the uncertainty of the coefficients and the corresponding models. With an increasing value of nb there was sometimes a pole in the origin and that is why the results might be unreliable. At very high values of nb there was a warning of an almost singular matrix. To avoid all these problems a low order model was preferred.

6.2.5 Response to applied wheel force

Frequency analysis was carried out on Saab 2000 in an approach flight condition at V_{REF} using the type design configuration. The effect of leaving out the vortex generators was investigated using the official aerodynamic data as well as CFD derived data. Computations were also made varying aileron control system friction and damping, control system stiffness and airplane rolling moment of inertia. A high speed flight case was also studied in a typical cruise flight case. For comparison Saab 340 was analyzed in the type design configuration as well as with zero friction and damping in the aileron control system. The computed results, derived with Fourier analysis, spectrum analysis and system identification using an ARX model, agree well almost up to the maximum input signal frequency of 2 Hz.

The frequency analysis results were different on the responses of aileron deflection, airplane roll rate and roll acceleration. The airplane pilot is not primarily interested in the movement of the ailerons. In steady conditions the pilot´s main concern is to get an adequate roll rate with the applied wheel force. In gusty conditions a sufficient roll acceleration is of interest when continuous corrections are needed. Airplane rolling moment of inertia had no effect on the response of aileron deflection to the applied wheel force, because the airplane inertia does not affect the pilots ability to move the ailerons. The effect of rolling moment of inertia was felt directly on the roll acceleration response. An effect was also noticed on airplane roll rate response, indicating that a steady state roll was not reached in the maneuver.

The frequency analysis results, obtained with the ARX model in the approach flight case, are summarized in figure 27, in which the response of airplane roll acceleration to the applied wheel force is presented. The amplitude gain on Saab 340 with type design

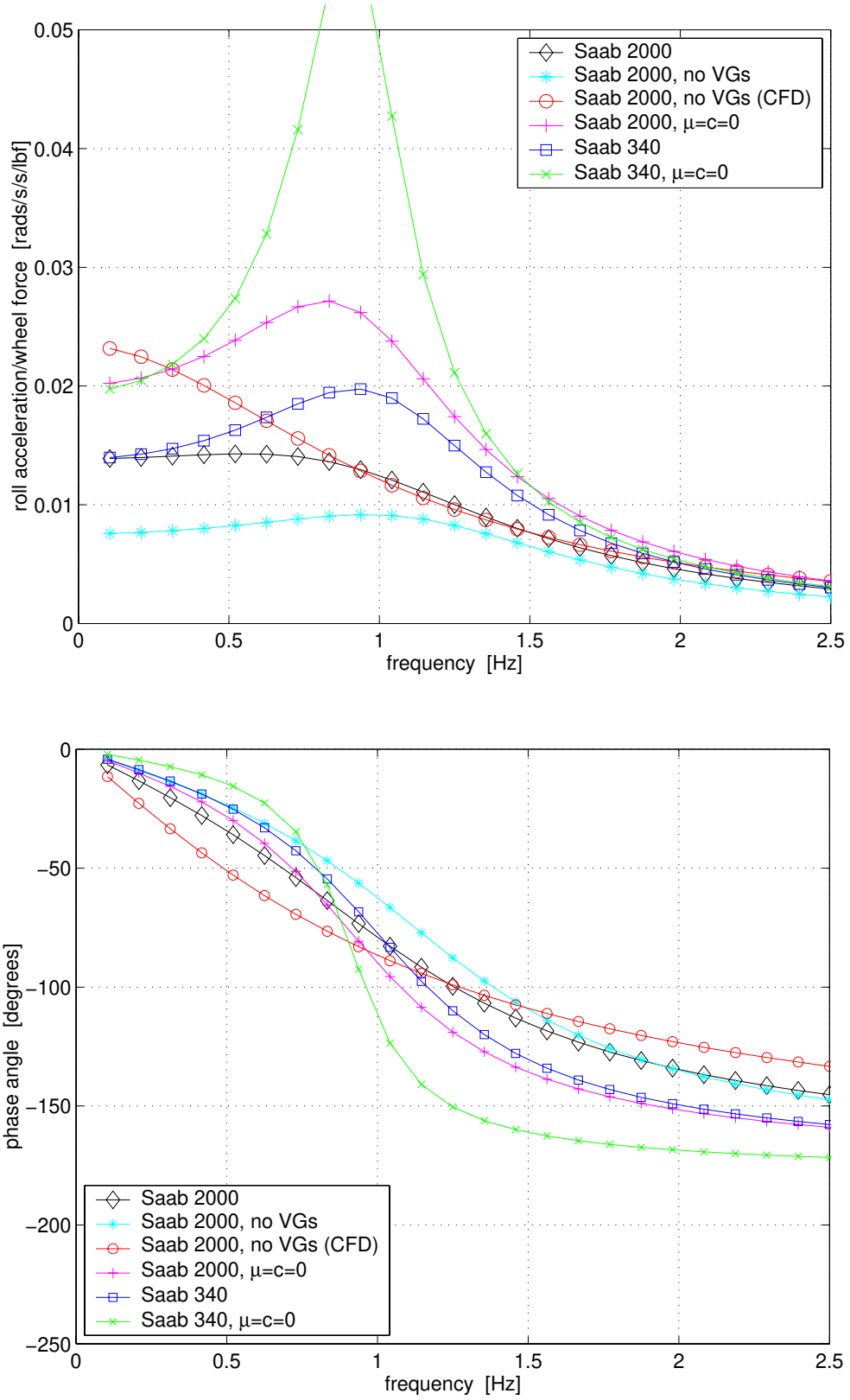

Figure 27. Frequency response of roll acceleration amplitude and phase angle to applied wheel force on Saab 340 and 2000 airplanes (ref. 59).

aileron showed a maximum at a frequency of 0.9 Hz, which is known to be in the region of pilot operation in gusty conditions. Saab 2000 with type design aileron showed a decreasing gain with increasing frequency without a resonance peak. Phase lags were somewhat larger on 2000 than on 340. Aileron deflection lagged the cockpit-control force input on Saab 2000 more than the 30^{o} limit value, specified in MIL Spec (ref. 43) for flying quality level 2 in Terminal Flight Phase C (which includes approach). At level 2 the flying qualities are adequate to accomplish the mission flight phase, but some increase in pilot workload or degradation in mission effectiveness, or both, exists. The lower limit of level 2 corresponds to Cooper-Harper rating 6.5 which is just barely certifiable. The MIL Spec requirement was fulfilled for Saab 340. The details above give an impression that dynamic aileron control is somewhat better and associated pilot work load somewhat lower on Saab 340 than on Saab 2000.

The effect of control system friction and damping is larger on Saab 340 than on 2000, partly because the basic friction on 340 is inherently higher due to a higher tension of the control cables. The main reason for the difference is however the remaining aerodynamic damping. Due to the airplane larger size and the small difference in V_{MCL} the aerodynamic damping moment on aileron hinge axis is a factor 2.6 higher on Saab 2000. The control system friction values in the airplane digital model have been established by system identification in ground response tests. However, it is known that the friction airborne is generally lower than on the ground. Thus the difference between the two airplanes may be larger than indicated by the curves based on nominal friction.

The frequency analysis on Saab 2000 without vortex generators, based on the official aerodynamic data, showed reductions in the amplitude gains of airplane roll rate and roll acceleration in the entire frequency band from 0 to 2.5 Hz. Without the vortex generators the amplitude gain of roll acceleration was only 50% of the gain on Saab 340 at a frequency of 1 Hz, which is known to be roughly the frequency of pilot operation. This is probably a reason for the high pilot work load initially experienced on Saab 2000 without vortex generators in turbulent approach conditions. The frequency analysis on 2000 without VGs, based on CFD computations, showed the reduction of gain on roll acceleration around 1 Hz compared with Saab 340. However, especially at low frequencies the results did not match the curve of Saab 2000 without vortex generators based on the official aerodynamic data. The simulation time histories did however give a warning of aileron overbalancing.

The effect of the aileron control system stiffness on Saab 2000 was investigated by increasing the stiffness to equal the 340 values. This brought practically no changes in the frequency response results indicating that the mechanical design of 2000 aileron control system is as good as the 340 system from the control point of view.

The frequency analysis on Saab 2000 in the cruise flight case showed that the gain of aileron deflection response was radically reduced due to the higher wheel forces at the higher speed. However, the gains of airplane roll rate and roll acceleration showed an increase at higher frequencies indicating that the high dynamic pressure would already give roll authority at the associated small deflections.

7. SUMMARY

Major achievements and most important findings of this thesis are:

An accurate modeling of the grid around the airfoil trailing edge is essential, because the fulfillment of the Kutta condition governs the creation of lift. Airfoil pitching moment and aileron hinge moment are especially sensitive to the flow conditions at the trailing edge due to the long moment arm to the reference points. The modeling of the slot is important as the flow and pressure distributions are sensitive to small geometry changes. Even relatively small changes in the pressure distribution have an influence on the hinge moment of a balanced aileron.

A methodology was established by grid variations for grid creation on slotted ailerons regarding the size and number of cells as well as stretching. The variations included the size of the computational domain, the size of the first cell in wall normal direction and the streamwise length of the cell in the corners of the slot and the trailing edge and in the vicinity of the stagnation point on the aileron. Grid convergence was studied with computational grids at four consecutive grid levels and at infinite grid level using Richardson´s extrapolation. The convergence studies confirmed a sufficient resolution of the created grids.

The convergence of the runs was ensured by monitoring the aerodynamic coefficients and the rms values of the time derivatives of the density and turbulent kinetic energy residuals. The hinge moment coefficient showed the slowest convergence being sensitive to the flow conditions at the trailing edge due to the long moment arm from the trailing edge to the hinge axis. The derivatives of the residuals were not good indicators of convergence due to the small local time steps. Consequently it is important to monitor the parameter of primary interest.

The review on the design experience on Saab 2000 shows that highly aerodynamically balanced ailerons pose a stringent design case. Quite a number of factors within aileron aerodynamics and dynamics, control system mechanics and pilot ergonomics set contradictory requirements. If some requirements are overlooked or stressed too much penalties can arise or the development time may increase considerably. The increased aileron chord together with the upwards bent aileron fixed trailing edge and tab caused a dip in the lift distribution with an associated increase of the airplane drag by 2% in cruise condition.

The fact that the performed low speed wind tunnel tests on a complete airplane model did not produce reliable data on aileron hinge moments due to scale effects was noticed late in the aircraft project when flight test data was available. The comparison of the CFD based results, derived within this work, showed a good agreement with flight test data. Hence CFD, together with a conversion to three-dimensional values, offers a new method for determining aerodynamic data for ailerons.

The CFD computations showed that the variation of the tab slot gap size had only a negligible effect on aileron efficiency and hinge moment. The variation of the aileron slot within the allowable production tolerances caused noticeable variations in aileron efficiency and hinge moment. The increase of the aileron slot gap size steepened the net hinge moment curve and thus increased the wheel forces. Increased aileron slot gap size caused a local flow separation on the aileron in front of the tab which may cause oscilla-

tion of the ailerons.

The combined analysis with CFD of aerodynamic data together with flight mechanical simulations showed a tendency to aileron overbalancing without vortex generators in steady heading sideslips and low speed roll maneuvers for the type design geared tab configuration. The variation in wheel force due to the effect of the vortex generators was considerably lower for a spring tab configuration. At high speed the spring tab rather than the geared tab configuration could much better compensate for the effect of speed and vortex generators. In roll maneuvers at high speed with the geared tab the effect of production tolerances on aileron slot gap size somewhat exceeded the variation due to the allowed tab rigging tolerances. With the spring tab configuration the same effect was considerably smaller.

Frequency analysis on the airplane roll acceleration response to the applied wheel force showed in an approach flight condition that Saab 340 has a resonance peak around 0.9 Hz, which is in the region of pilot operation in gusty conditions. Due to an inherently higher aerodynamic damping Saab 2000 does not have this peak. Frequency analysis, based on pertinent aerodynamic data without vortex generators, showed on 2000 a further reduction in the gain of airplane roll acceleration response to the applied wheel force. Aileron deflection lagged the cockpit-control force input on Saab 2000 more than on Saab 340. This is probably why the pilot work load on Saab 2000 was initially experienced high in turbulent approach conditions.

In conclusion the combination of CFD with flight mechanical simulations is a promising tool for the preliminary design of ailerons. Future work would be needed to better validate the two-dimensional CFD computations for an aerodynamically balanced aileron. A two-dimensional wind tunnel test on a balanced control surface is then needed at representative Reynolds and Mach numbers.

REFERENCES

1. Althaus D., Stuttgarter Profilkatalog I, Institut fur Aerodynamik und Gasdynamik der Universität Stuttgart, 1972, 386 p.

2. Ashby D., Experimental and Computational Investigation of Lift-Enhancing Tabs on a Multi-Element Airfoil, Stanford University JIAA TR 116, June 1996, 199 p.

3. Ashour S. S., Investigation of New Methods for the Integration of Stiff Ordinary Differential Systems, University of California, Santa Barbara 1989.

4. Bergmeyer P., Aerodynamic development of Fokker F28 wing- Flap, lift dumpers and lateral control, DE INGENIEUR, VOL. 81, P. L 94-L 100, 1969, 7 p.

5. Bergström J., Functional description of the FORMIC State Space Model environment, Saab Report 73FMS4183, 990117, 5 p.

6. Boermans L.M.M., Selen H.J.W., On the design of some airfoils for sailplane application, Delft University of Technology, Department of Aerospace Engineering, April 1981, 48 p.

7. Bufacchi B., Lucchesini M., Manfriani L., Valtorta, E., Aerodynamic control design: Experience and results at Aermacchi, In AGARD, Aerodynamics of Combat Aircraft Controls and of Ground Effects, 1990, 13 p.

8. Cebeci T., Bradshaw P., Momentum Transfer in Boundary Layers, McGraw-Hill/ Hemispehere, Washington D.C., 1977.

9. Chalk C. R., Neal T. P., Harris T. M., Pritchard F. E., Woodcock R. J., Background information and User Guide for MIL-F-8785B(ASG), “Military Specification - Flying Qualities of Piloted Airplanes”, Tech. Rep. AFFDL-TR-69-72, Air Force Flight Dynamics Lab., Wright-Patterson Air Force Base, Aug. 1969, 684 p.

10. Chin V. D., Dominik C. J., Lynch F. T., Rodriguez D. L., 2-D aileron effectiveness study, In AGARD, A Selection of Experimental Test Cases for the Validation of CFD Codes Volume 2, AGARD-AR-303-VOL-2, 1994, 20p.

11. Cooper G. E., Harper R. P., The Use of Pilot Rating in the Evaluation of Aircraft Handling Qualities, NASA TN D-5153, 1969, 52 p.

12. de Cock K. M. J., Lindblad I., 2D Maximum lift prediction for the 59 percent span wing section of the A310 aircraft, High Lift Aerodynamics, phase IV, Garteur/TP-098-**, AG 25, March 23 1998, 174 p.

13. Design Objectives for Handling Qualities of Transport Aircraft, Aerospace Recommended Practice ARP 4104, Society of Automotive Engineers Inc., July 1988, 23 p.

14. DeYoung J., Harper C.W., Theoretical Symmetric Span Loading at Subsonic Speeds for Wings having Arbitrary Plan Form, NACA-TR-921, 1948, 56 p.

15. Dini P., Selig M. S., Maughmer M. D., Simplified Linear Stability Transition Prediction Method for Separated Boundary Layers, AIAA Journal, Vol. 30, No. 8, August 1992, p. 1953...1961.

16. Drela M., A User´s guide to MSES 2.7, MIT Computational Aerospace Sciences Laboratory, November 1994, 28 p.

17. Drela M., Giles M. B., Viscous-Inviscid Analysis of Transonic and Low Reynolds

Number Airfoils, AIAA Journal, Vol. 25, No. 10, October 1987.

18. Drela M., Two-dimensional transonic aerodynamic design and analysis using the Euler equations, Dissertation at Massachusets Institute of Technology, 851202, 159 p.

19. Dunn O. R., Aerodynamically Boosted Surface Controls and their Application to the DC-6 Transport, Douglas Aircraft Company Inc., Santa Monica Plant, Second International Conference I.A.S and R.Ae.S, New York 1949, 39 p.

20. Engineering Sciences Data Item Controls 04.01.01, Rate of Change of Hinge-Moment Coefficient With Incidence For A Plain Control In Incompressible Two-Dimensional Flow, $(b_1)_0$, With Amendments A and B, August 1989, 4 p.

21. Engineering Sciences Data Item Controls 04.01.02, Rate of Change of Hinge-Moment Coefficient With Control Deflection For A Plain Control In Incompressible Two-Dimensional Flow, $(b_2)_0$, With Amendments A and B, August 1989, 4 p.

22. Engineering Sciences Data, Aerodynamics, Volume 5 Controls and Flaps, ESDU International.

23. Etkin B., Dynamics of Atmospheric Flight, John Wiley & Sons Inc., 1972, 579 p.

24. Etkin B., Dynamics of Flight, John Wiley & Sons Inc., 1958, 513 p.

25. Ewaldsson S., Saab 2000 Certification Basis, Saab AB Directive 73CCS0016 Amd 6, 930218, 624 p.

26. Federal Aviation Regulations Part 25, Airworthiness Standards: Transport Category Airplanes, Department of Transportation, Federal Aviation Administration.

27. Filisetti A., Ferretti G., Considerations on the manual flight control design of a military transport aircraft, In AGARD Stability and Control, 1972, 20 p.

28. Halfmann G., Jonas K., The design of control forces and their adaptation in a flight test, taking into account the example of the DO 228, IN: Problems and development trends in general aviation; Symposium, Friedrichshafen, West Germany, March 24, 25, 1983, Deutsche Gesellschaft fuer Luft- und Raumfahrt, p. 165-191.

29. Glauert H., Theoretical Relationships for an Aerofoil with Hinged Flap, Aeronautical Research Council, R. & M. No. 1095, 1927, 15 p.

30. Grismer M., Kinsey D., Grismer D., Hinge Moment Predictions Using CFD, AIAA Paper 2000-4325, 18th AIAA Applied Aerodynamics Conference, 14-17 August 2000, Denver CO, 13 p.

31. Jiang F., CFD Predictions for Control Surface Effectiveness, AIAA Paper 2000-0510, 38th Aerospace Sciences Meeting & Exhibit, 10-13 January 2000, Reno NV, 11 p.

32. Joint Airworthiness Requirements, JAR-25, Large Aeroplanes, Change 13.

33. Kvarnström J., Flying Qualities Design Targets - Civil Transport Type of Airplanes, Saab AB Specification 73FMS0020, 901001, 28 p.

34. Larsson T., Separated and High-lift Flows over Single and Multi-element Airfoils, ICAS paper 94-5.7.3, Sept. 1994, 14 p.

35. Larsson T., 2D Turbulent Navier-Stokes Computations for the Saab 2000 Stabilizer, Saab Technical Report TURLU11-9305, 931222, 23 p.

36. Ljung L., Glad T. Model construction and simulation (Modellbygge och simulering), Studentlitteratur 1991, 363 p. (in swedish)

37. Mai H.U., Generalizations of extended lifting line theory and computer program LIFLI for the calculation of lift distribution of wing and wing-body configurations, Helsinki University of Technology, Laboratory of Aerodynamics Report 78-B1, 1978, 57 p. (in finnish)

38. Marsden D.J., Wind Tunnel Tests of a Slotted Flapped Wing Section, Canadian Aeronautics and Space Journal, Vol. 24 No. 2, March/April 1978, p. 83...91.

39. Masefield O. L. P., Aerodynamic design of a manual aileron control for an advanced turboprop trainer, ICAS Congress Jerusalem Aug. 28-Sept. 2, 1988, 8 p.

40. Masefield O. L. P., Design of a manual roll control for a trainer aircraft, A Doctoral Thesis, Loughborough University of Technology, 1990, 218 p.

41. McGhee R. J., Beasley W. D., Low-Speed Aerodynamic Characteristics of a 13-Percent-Thick Medium-Speed Airfoil Designed for General Aviation Applications, NASA Technical Paper 1498, 1979, 76 p.

42. Military Standard Flying Qualities of Piloted Vehicles, MIL-STD-1797A, USA Department of Defence, 1991.

43. Military Specification, Flying Qualities of Piloted Airplanes, MIL-F-8787C, NOTICE 1, 24 September 1991, 31 p.

44. Moran J., An Introduction to Theoretical and Computational Aerodynamics, John Wiley & Sons, 1984, 464 p.

45. Morgan M. B., Bethwaite C. F., Nivison J., Spring-tab controls - notes on development to date, with special reference to design aspects, Royal Aircraft Establishment, Farnborough, Report No. Aero 1972, September 1944, 89 p.

46. Morgan M. B., Thomas H. H. B. M., Control Surface Design in Theory and Practice, The RAeS Journal, 1945, p. 431... 510.

47. Morris D. E., Designing to avoid dangerous behavior of an aircraft due to the effects on control hinge moments of ice on the leading edge of the fixed surface, ARC C.P. No. 66, Royal Aeronautical Establishment, 1947, 10 p.

48. Rizzi A., Vos J., Toward Establishing Credibility in Computational Fluid Dynamics Simulations, AIAA Journal, Vol. 36 No. 5, 1998, p. 668...675.

49. Roache P., Verification of Codes and Calculations, AIAA Journal, Vol. 36 No. 5, 1998, p. 696...702

50. Råde L., Westergren B., Beta β Mathematics Handbook, Concepts Theorems Methods Algorithms Formulas Graphs Tables, Studentlitteratur Chartwell-Bratt, Second edition 1990, 494 p.

51. SAAB 340-2000 Certification Review Item CRI Number B01, Joint Aviation Authorities, Amendment 6 to Saab Report 73CCS0016, 910430, 3p.

52. Schlichting H., Boundary Layer Theory, McGraw-Hill 1979, 817 p.

53. Sears R. I., Wind-Tunnel Data on the Aerodynamic Characteristics of Airplane Control Surfaces, NACA ACR No. 3L08, 1943, 215 p. (also published as NACA WR L-663).

54. Soinne E., Aerodynamically Balanced Aileron Design, Royal Institute of Technology, Department of Aeronautics Report 98-37, 1998, 94 p.

55. Soinne E., Analysis of FX 61-163 Airfoil with MSES Program, Royal Institute of Technology, Department of Aeronautics Report 97-3, 1997, 44 p.

56. Soinne E., Dimensioning Cases for the Aileron Design of a Commercial Aircraft, Royal Institute of Technology, Department of Aeronautics Report 97-25, 1997, 37 p.

57. Soinne E., Effects of Tolerances on Aerodynamically Balanced Ailerons, Royal Institute of Technology, Department of Aeronautics Report 2000-7, 2000, 172 p.

58. Soinne E., Evaluation of Navier-Stokes program NS2D for a low speed airfoil, Royal Institute of Technology, Department of Aeronautics Report 97-2, 1997, 53 p.

59. Soinne E., Flight Mechanical Design of Aerodynamically Balanced Ailerons, Royal Institute of Technology, Department of Aeronautics Report 99-16, 1999, 145 p.

60. Soinne E., Literature review on Aileron Design, Royal Institute of Technology, Department of Aeronautics Skrift 97-17, 1997, 25 p. + App. 125 p.

61. Soinne E., Validation of CFD Computations on Control Surfaces, Royal Institute of Technology, Department of Aeronautics Report 98-15, 1998, 83 p.

62. Soinne E., Validation of Navier-Stokes Computations and a Transition Model, Royal Institute of Technology, Department of Aeronautics Report 99-15, 1999, 56 p.

63. Somers D. M., Experimental and Theoretical Low-Speed Aerodynamic Characteristics of a Wortmann Airfoil as Manufactured on a Fiberglass Sailplane, NASA TN D-8324, 1977, 48 p.

64. Toll T. A., Summary of lateral-control research, NACA-TR-868, 1947, 74p. (Also published as NACA TN No. 1245)

65. USAF Stability and Control DATCOM, Airforce Flight Dynamics Laboratory, Wright-Patterson Air Force Base Ohio, Revised February 1972, Section 6.1.3, Section Hinge Moment of High-Lift and Control Devices.

66. Vos J.B., Leyland P., Lindberg P.Å., van Kemenade V., Gacherieu C., Duquesne N., Lötstedt P., Weber C., Ytterström A., NSMB Handbook 4.0, February 13th 1997, 185 p.

67. Weissinger J., Über die Auftriebsverteilung von Pfeilflügeln, Forsch.-Ber. d. Zentr. f. Wiss. Berichtswesen, No. 1553, Berlin-Adlershof, 1942.

68. Weissinger J., Über eine Erweiterung de Prandtlschen Theorie der tragenden Linie, Mathematische Nachrichten, 2. Band, 1949, p. 45...106

69. Wentz W. H., Wind Tunnel Force and Pressure Tests of a 13% Thick Medium Speed Airfoil With 20% Aileron, 25% Slotted Flap and 10% Slot-Lip Spoiler, NASA Contractor Report 3439, 1981, 113 p.